The number fraction of iron-containing particles affects OH, HO$_2$ and H$_2$O$_2$ budgets in the atmospheric aqueous phase

Amina Khaled[1], Minghui Zhang[1], and Barbara Ervens[1]

[1]Université Clermont Auvergne, CNRS, SIGMA Clermont, Institut de Chimie de Clermont-Ferrand, 63000 Clermont-Ferrand, France

Correspondence: Barbara Ervens (barbara.ervens@uca.fr)

Abstract. Reactive oxygen species (ROS), such as OH, HO$_2$ and H$_2$O$_2$ ~~),~~ affect the oxidation capacity of the atmosphere and cause adverse health effects of particulate matter. The role of transition metal ions (TMIs) in impacting the ROS concentrations and conversions in the atmospheric aqueous phase has been recognized for a long time. Model studies usually assume that the total TMI ~~concentration~~ mass as measured in bulk aerosol or cloud water samples is distributed equally across all particles or droplets. This assumption is contrary to single-particle measurements that have shown that only a small number fraction of particles contain iron and other TMIs ($F_{N,Fe}$ < 100%) which implies that also not all cloud droplets contain TMIs. In the current study, we apply a box model with an explicit multiphase chemical mechanism to simulate ROS formation and cycling in ~~(i)~~ aqueous aerosol particles and ~~(ii)~~ cloud droplets. Model simulations are performed for the range of 1% $\leq F_{N,Fe} \leq$ 100% for constant pH values of 3, 4.5 and 6 and constant total iron mass concentration (10 or 50 ng m$_{air}^{-3}$). Model results are compared for two sets of simulations with $F_{N,Fe}$ < 100% (~~FeN~~ Fe textsubscriptN<100) and 100% (FeBulk). We find largest differences between model results in OH and HO$_2$/O$_2^-$ concentrations at pH = 6. Under these conditions, HO$_2$ is subsaturated in the aqueous phase because of its high effective Henry's law constant and the fast chemical loss reactions of the O$_2^-$ radical anion. As the main reduction ~~of~~ process of Fe(III) is its reaction with HO$_2$/O$_2^-$, we show that the HO$_2$ subsaturation leads to ~~predicted~~ Fe(II)/Fe(total) ratios for $F_{N,Fe}$ < 100% that are lower by a factor of $\leq$ 2 as compared to bulk model approaches. This trend is largely independent of the total iron concentration, as both chemical source and sink rates of HO$_2$/O$_2^-$ scale with the iron concentration. ~~The chemical radical (OH, HO$_2$) loss in particles is usually compensated by its uptake from the gas phase.~~ We compare model-derived reactive uptake parameters ~~γ(OH) and γ(HO$_2$)~~ γ_{OH} and γ_{HO2} for the full range of $F_{N,Fe}$. While ~~γ(OH)~~ γ_{OH} is not affected by the iron distribution, the calculated ~~γ(HO$_2$)~~ γ_{HO2} range from 0.0004 to 0.03 for $F_{N,Fe}$ = 1% and 100%, respectively. Implications of these findings are discussed for the application of lab-derived ~~γ(HO$_2$)~~ γ_{HO2} in models to present reactive HO$_2$ uptake on aerosols. ~~As the oxidant budget in aerosol particles and cloud droplets is related to the oxidative potential, we also~~ We conclude that the iron distribution ($F_{N,Fe}$) should be taken into account to estimate the ROS concentrations and ~~health impacts~~ oxidation potential of particulate matter that might be overestimated by bulk sampling and model approaches. Our study suggests that the number concentration of iron-containing particles $F_{N,Fe}$ may be more important than the total iron mass concentration in determining ROS budgets and uptake rates in cloud and aerosol water.

1 Introduction

The main oxidants in the atmospheric aqueous phases of cloud and aerosol particles include the hydroxyl radical (OH) and hydrogen peroxide (H_2O_2 ~~H_2O_2~~) whose concentration levels are closely linked to the hydroperoxy radical (HO_2 ~~HO_2~~/O_2^- ~~O_2^-~~). The concentrations of these reactive oxygen species (ROS) are influenced by various redox reactions of transition metal ions (TMIs).

30 Iron is the most abundant TMI in aerosol particles and cloud water. Its main sources include dust and coal combustion (Moffet et al., 2012) and biomass burning (Wang et al., 2015). Its concentration in cloud water ranges from nano- to micromolar levels (Cini et al., 2002; Deguillaume et al., 2005). Iron mass concentrations in aerosol samples reach from less than 1 ng m^{-3} to more than 100 ng m^{-3} (Schmücke, Germany) and sometimes up to several hundred ng m^{-3} at other continental locations (~~Fomba et al. (2015)~~ (Fomba et al., 2015) and references therein).

35 The role of transition metal ions in affecting the ROS concentration levels and redox reactions in clouds and particles has been explored in many model, lab and field studies, e.g., Deguillaume et al. (2004, 2005); Mao et al. (2013). Reactions of iron and other TMIs (e.g., copper) in the atmosphere have also been linked to the oxidative potential of particulate matter, causing oxidative stress in the respiratory tract and lungs (Saffari et al., 2014; Arangio et al., 2016; Tong et al., 2016; Molina et al., 2020; Wei et al., 2021). In particular, the ~~Fenton reaction, the~~ oxidation of iron(II) by hydrogen peroxide (Fenton reaction) has

40 been identified as one of the main chemical sources of the OH radical in cloud water (Ervens et al., 2003; Deguillaume et al., 2004; Tilgner et al., 2013), aqueous phase aerosol particles (Al-Abadleh, 2015) and lung fluid (Charrier et al., 2015).

TMI concentrations in the cloud and aerosol phases are usually reported based on bulk measurements representing the total TMI mass per aqueous or gas phase volumes. However, single-particle analyses have shown that iron is only present in a small number fraction of particles~~.~~: Furutani et al. (2011) found that up to 15% of particles in the diameter range between 0.5 and 1

45 μm contain iron~~(Zhang et al., 2014)~~. Similar number fractions (< 1 – 15%) were observed in Shanghai, where air masses were also affected by dust storms or biomass and coal burning (Zhang et al., 2014). A similar size range for iron-containing particles but smaller average number fraction (∼4%) were found above the English Channel in air masses affected by steel works (Choël et al., 2007). As particles in this size range commonly act as cloud condensation nuclei (CCN), these analyses suggest that not all cloud droplets contain iron and that also the measured iron mass concentration in aerosol populations is not equally

50 distributed among all particles. Drop-size-resolved cloud water measurements at a continental background site have shown that iron and copper are present in the same drop size range whereas manganese is more abundant in larger droplets (Fomba et al., 2015). This may suggest that CCN were comprised of internal mixtures of iron and copper whereas manganese-containing particles were externally mixed and of different hygroscopicity and/or different sizes.

The oxidation state of iron ~~affect~~ affects its solubility and thus its bioavailability and biogeochemical cycles in the atmosphere

55 and oceans. Generally, ferrous salts are more soluble than ferric salts, with increasing solubility under acidic conditions, e.g., Ingall et al. (2018). Results from a global ~~aerosol~~ model study revealed large differences in predicted and observed iron solubility; observed Fe(II)/Fe(total) ratios were on average between ∼1 and ∼10% with larger variability in coarse than in

fine particles (Luo et al., 2005). The Fe(II) fractions in particle samples above oceans has been shown to be above 30% - 75% (Ingall et al., 2018). Measurement of the Fe(II)/Fe(total) ratio on a single particle basis revealed ratios of ≤20% for particles from various sources (Takahama et al., 2008). In cloud water, Fe(II) often dominates the total iron ~~in cloud water~~concentration, in particular during day-time when iron(III) hydroxy and organo complexes are reduced by photolysis processes (Deguillaume et al., 2005).

Multiphase chemistry models are usually initialized with bulk concentrations of iron to make predictions on the role of aqueous phase chemistry on ROS levels (e.g., Ervens et al. (2003); Tilgner et al. (2013); Tong et al. (2017)), sulfate formation (e.g., Alexander et al. (2009); Chang et al. (1987)) or iron deposition (Myriokefalitakis et al., 2018). In a previous model study, we have demonstrated that such bulk approaches may not be appropriate for highly reactive compounds as redistribution and diffusion processes among droplets of chemical composition might lead to non-linear effects impacting concentration levels (Khaled et al. (2021)). While that study was focused on the biodegradation of organics by bacteria~~that~~, which are only present in a small number fraction of cloud droplets, we apply the same idea in the present study to the ROS cycling dependent on the number fraction of iron-containing particles.

We perform box model simulations ~~a box model~~ with a detailed gas and aqueous phase chemical mechanism, in which a constant iron mass concentration m_{Fe} [ng m$_{air}^{-3}$] is distributed to a fraction of (i) cloud droplets or (ii) aqueous aerosol particles. We investigate the conditions in terms of pH, iron distribution and total iron mass, under which the number fraction of iron-containing particles significantly affects the concentration levels and phase transfer of OH, HO$_2$ and H$_2$O$_2$ in the atmospheric multiphase system. We discuss the potential implications of these effects for the interpretation of measurements and model studies of the iron oxidation state, radical uptake rates onto aqueous aerosol particles and ROS budgets and oxidative potentials of aerosol and cloud water.

2 Multiphase box model

2.1 Model description

We use a box model with detailed gas and aqueous phase chemical mechanisms. The gas-phase chemical mechanism with 58 reactions is based on the NCAR Master Chemical Mechanism (Madronich and Calvert, 1989). The aqueous phase chemical mechanism includes 43 reactions (Ervens et al., 2008; Tong et al., 2017) (Tables S1 - S3 in the supplement). Phase transfer processes for 14 species are described kinetically based on the resistance model (Schwartz, 1986; Nathanson et al., 1996) (Table S4). The model uses the standard equations for multiphase processes (Seinfeld and Pandis, 1998):

$$\frac{dC_{aq}}{dt} = \underbrace{k_{mt}\, LWC \left(C_g - \frac{C_{aq}}{LWC\, K_{H(eff)}\, R\, T} \right)}_{phase\ transfer\ rate} + \underbrace{S_{aq} - L_{aq}}_{chem\ rate} \tag{1}$$

$$\frac{dC_g}{dt} = \underbrace{-k_{mt}\,LWC\left(C_g - \frac{C_{aq}}{LWC\,K_{H(eff)}\,R\,T}\right)}_{phase\ transfer\ rate} + \underbrace{S_g - L_g}_{chem\ rate} \tag{2}$$

whereas both the gas phase (C_g) and aqueous phase (C_{aq}) concentrations are expressed in units of mol g_{air}^{-1}, *LWC* is the liquid water content [vol/vol], $K_{H(eff)}$ is the (effective) Henry's law constant, and S_{aq}, S_g and L_{aq}, L_g are the chemical source and loss rates in the aqueous and gas phases [mol $g_{air}^{-1}s^{-1}$]. *R* and *T* are the constant for ideal gases (0.082058 L atm (K mol)$^{-1}$) and absolute temperature [K]. The mass transfer coefficient k_{mt} [s^{-1}] is defined as

$$k_{mt} = \left(\frac{r_d{}^2}{3\,D_g} + \frac{r_d}{3\,\alpha}\sqrt{\frac{2\pi\,M_g}{R\,T}}\right)^{-1} \tag{3}$$

whereas r_d is the drop radius, D_g the gas phase diffusion coefficient, α the mass accommodation coefficient, and M_g the molecular weight. The mass transfer coefficient k_{mt} takes into account gas phase diffusion and the mass accommodation, i.e. the probability that a molecule that hits the droplet (or particle) surface is taken up. It is the inverse of the characteristic time for these two resistances. Its full derivation can be found in the literature, e.g. by Nathanson et al., 1996, and is therefore not repeated here. In our model studies, it is assumed that all solutes are homogeneously mixed and no concentration gradients exist between the gas/aqueous interface and the bulk of the aqueous phase. This assumption is justified if chemical loss processes in the aqueous phase are comparatively slow, so that aqueous phase diffusion can evenly distribute the species throughout the aqueous volume. The competition between aqueous phase diffusion and chemical loss in the aqueous phase is commonly quantified by the dimensionless diffuso-reactive parameter q (Equation S.3 in the Supplement, Seinfeld and Pandis (1998)). This parameter does not take into account chemical sources within the aqueous phase. As discussed in a previous study, the Fenton reaction can act as a such a source for the OH radical in aqueous solution (Ervens et al., 2014). A detailed comparison and discussion of the parameter q and the role of aqueous phase diffusion can be found in the Supplement (Section S2). The box model considers monodisperse cloud droplet or wet aerosol particle populations with constant diameters (*D*) of 20 μm for cloud droplets and 300 nm for aqueous aerosol particles, respectively. The simulations are run at constant temperature (285.6 K), pressure (9.21·10^4 Pa) and air density (1.31·10^{-3} g cm^{-3}).

2.2 Model simulations

The schematic of the model setup together with the main ROS formation and conversion processes are shown in Fig. 1. Results of two model approaches will be compared:

– a) **FeBulk**: All droplets (particles) have the same chemical composition. The iron concentration is identical in all droplets (particles). The fraction of iron-containing droplets (particles) is $F_{N,Fe} = 100\%$.

- b) **FeN<100**: A subset of the number concentration (N) of droplets (or particles) is initialized with iron whereas the remainder of the droplets (particles) is iron-free. In the base case simulations, we assume that the number fraction of iron-containing droplets (particles) is $F_{N,Fe}$ = 2%; $F_{N,Fe}$ is varied from 1 - 99% in sensitivity studies (Section 3.3).

We assume an iron mass concentration (m_{Fe} = 10 ng m$_{air}^{-3}$). (Some sensitivity studies for m_{Fe} = 50 ng m$_{air}^{-3}$ are discussed.) Therefore, in the FeN<100 approach, the aqueous phase iron concentration [M] is higher in the iron-containing droplets (particles) than in the FeBulk approach as the iron mass is distributed to fewer droplets (particles). Simulations are performed for constant values of pH = 3, 4.5 and 6. All model parameters are summarized in Table 1.

Gas phase species are initialized with the values in Table S5 and are not replenished throughout the simulations. Chemical and phase transfer rates are analysed after a simulation time of 400 seconds. This time scale refers approximately to the lifetime of a single cloud droplet. It can be estimated based on updraft and downdraft velocities a cloud droplet experiences and on cloud thickness (e.g., average vertical velocity of 0.5 m s^{-1} throughout cloud that is 100 m thick, as typical values for shallow stratocumulus clouds). To demonstrate that our results and conclusions do not strongly depend on the choice of the timescale, we compare the main source and loss processes of the three species at t = 400 s and t = 2000 s (Section 3.2). During even longer time scales, the concentrations may change in the box model; however, this may not be realistic since highly reactive gases are quickly depleted (e.g., SO$_2$) whereas in the real atmosphere, emissions might replenish them.
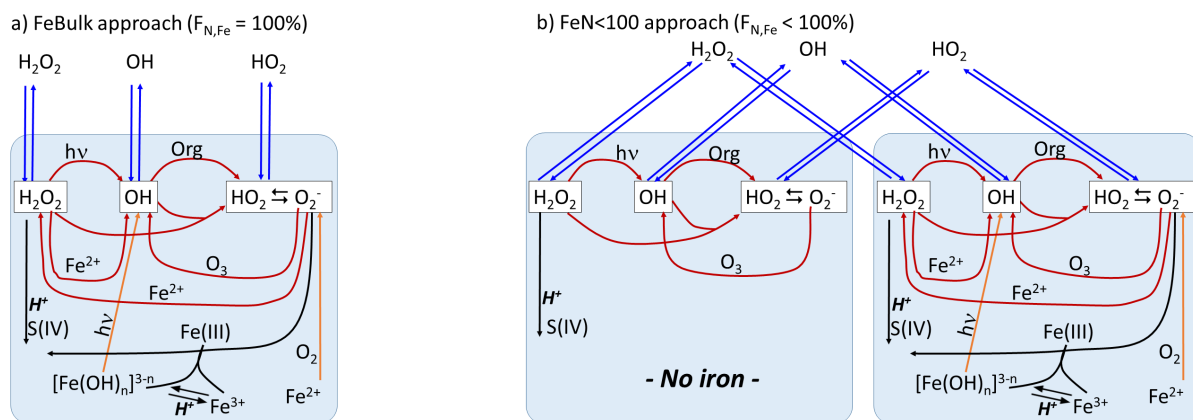
Figure 1. Model schematic: a) FeBulk: The total iron mass concentration (m_{Fe} = 10 ng m^{-3}) is equally distributed among all droplets or particles ($F_{N,Fe}$ = 100%), b) FeN<100: The same iron mass concentration is distributed among a subset of droplets or particles (base case: $F_{N,Fe}$ = 2%). Major ROS processes are phase transfer (blue), ROS net production (orange), ROS conversions (red) and ROS loss (black). Model parameters are summarized in Table 1.

Table 1. Model parameters for multiphase simulations for cloud droplet and aerosol populations. D = diameter, N = number concentration, LWC = liquid water content, ~~m_{Fe}~~ m_{Fe} = total iron mass concentration, $F_{N,Fe}$ = number concentration of droplets or particles that contain iron, $[Fe]_{aq}$ = aqueous phase concentration of iron. Numbers in parentheses denote values or parameter ranges of sensitivity studies~~; all other values are those of base case simulations~~.

Parameter	FeBulk	FeN<100	
Cloud droplets	All	Iron-free	Iron-containing
D / μm	20 (10, 40)	20 (10, 40)	20 (10, 40)
N / cm^{-3}	100	98 (99 - 1)	2 (1 - 99)
LWC / g m^{-3}	0.42	0.41 (0.416 - 0.042)	2 (0.042 - 0.416)
m_{Fe} / ng m^{-3}	10 (50)	0	10 (50)
$F_{N,Fe}$ / %	100	0	2 (1 - 99)
$[Fe]_{aq}$ / μM	0.41	0	21 (0.43 - 42)
Aerosol particles	All	Iron-free	Iron-containing
D / μm	0.3 (0.15, 0.6)	0.3 (0.15, 0.6)	0.3 (0.15, 0.6)
N / cm^{-3}	1500	1470 (1485 - 15)	~~2~~ 30 (15 - 1485)
LWC / μg m^{-3}	21	20.6 (20.8 - 0.3)	0.6 (0.3 - 20.8)
m_{Fe} / ng m^{-3}	10 (50)	0	10 (50)
$F_{N,Fe}$ / %	100	0	2 (1 - 99)
$[Fe]_{aq}$ / M	0.008	0	0.41 (0.00008 - 0.82)

3 Model results and discussion

3.1 Aqueous phase concentrations and rates

3.1.1 Cloud droplets

135 Figure 2 summarizes the ROS concentrations, and the chemical and phase transfer rates for the cloud case ~~(m_{Fe} = 10 ng m^{-3}, $F_{N,Fe}$ = 100% vs 2%,~~ at pH = 4.5~~, t = 400 s). The~~ ; the corresponding figures for simulations at pH = 3 and 6 are shown in Fig. S1 (Supplement). The net ~~rates of the phase transfer~~ transfer rates [mol $g_{air}^{-1} s^{-1}$] into the aqueous phase are shown in the yellow boxes. For FeN<100, the relative contributions [%] of this rate into the iron-free and iron-containing droplets are shown next to the arrows. ~~If the effect of the iron distribution across the droplet population were negligible, the ratio of these rates~~

140 ~~should be equal to the ratio of the LWCs of the two drop classes (98% : 2%).~~ The phase transfer rates are additionally shown in units of M s^{-1} ~~,~~ (using the air density of 1.13·10^{-3} g cm^{-3} and LWCs in Table 1), together with the chemical source and loss rates in the aqueous phase [M s^{-1}] and the corresponding aqueous phase ROS concentrations [M] (white boxes). If the effect of iron were negligible on aqueous phase concentrations and aqueous phase rates, there should be no ~~difference in these values in any of the~~ concentration difference between any droplets, neither between the results for FeBulk and FeN<100 nor between

145 the iron-free and iron-containing droplets. In addition, also the ratio of the phase transfer rates should be equal to the ratio of the LWCs of the two drop classes (98% : 2%).
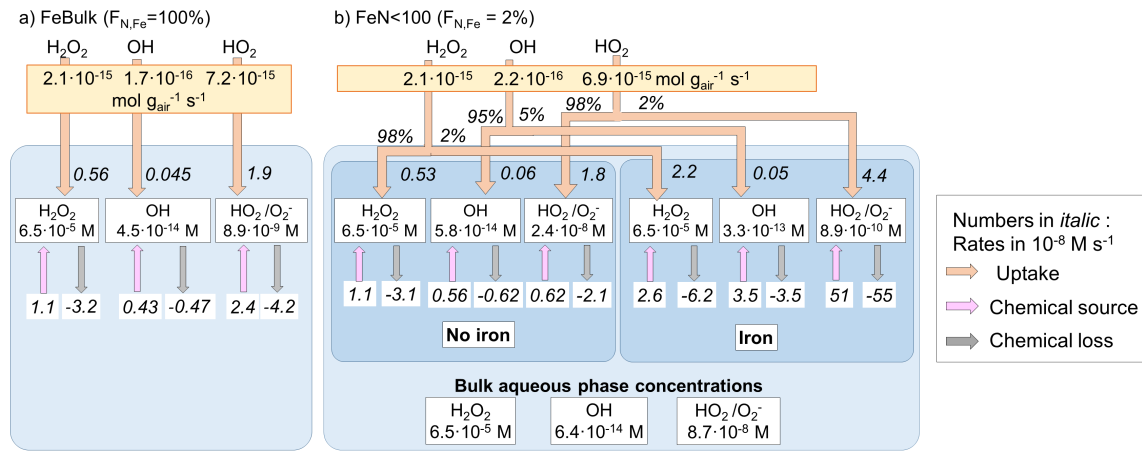
Figure 2. Multiphase scheme for cloud water showing the phase transfer and chemical source and loss rates in the aqueous phase, $m_{Fe} = 10$ ng m^{-3}, pH = 4.5. a) FeBulk approach, b) FeN<100 approach with a fraction of iron-containing droplets of $F_{N,Fe} = 2\%$. Numbers below the species names are aqueous phase concentrations [M], chemical and phase transfer rates are shown in M s^{-1}. Net phase transfer rates near the top of the figure are expressed in gas phase units [mol g$_{air}^{-1}$ s^{-1}]; the relative contributions [%] into the iron-free and iron-containing droplets are shown next to the arrows. The bulk concentrations ~~below~~ at the bottom of panel b) represent the ~~total ROS~~ bulk concentrations weighted by the contributions of the two droplet classes to total LWC (98% : 2%).

All ROS are predicted to be taken up into cloud water, independently of the iron distribution at pH = 4.5 () ~~. For all three ROS, the~~ Fig. 2) and also their ratio of the phase transfer rates are near the ratio of the LWCs of the two droplet classes (98% : 2%). Significant deviations from his theoretical value occur at pH = 3 for HO$_2$ (Fig. S1b) and at pH = 6 for H$_2$O$_2$ that is

150 predicted to evaporate from iron-free droplets (Fig. S1d).

The ~~uptake rates in M s^{-1} between FeBulk and the iron-free droplets in the FeN<100 approach are similar (e.g. for H$_2$O$_2$: 0.56 M s^{-1} and 0.53 M s^{-1}) whereas they are higher into the iron-containing droplets (2.2 M s^{-1}).~~

~~The H$_2$O$_2$~~ concentrations in all droplets ~~for~~ under all conditions and pH values (Fig. S1) correspond to the equilibrium concentrations according to Henry's law, in agreement with previous studies that have shown that H$_2$O$_2$ is at thermodynamic

155 equilibrium in cloud water (Ervens, 2015). ~~Accordingly, the partitioning coefficient ϵ is near unity for FeBulk and FeN<100 (a). It is defined as~~

$$\epsilon = \frac{C_{aq}}{p_g \cdot K_{H(eff)}} \tag{E.4}$$

~~with C_{aq} and p_g being the aqueous phase concentration Mand gas phase partial pressure atmand $K_{H(eff)}$ the (effective) Henry's law constant M atm^{-1}.~~

At pH = 3 and 4.5, the efficient H_2O_2 consumption is compensated by a relatively higher uptake rate, resulting in the efficient replenishment of H_2O_2 and ~~a constant (equilibrium) concentration.~~ equilibrium concentration. The uptake rates in M s^{-1} between FeBulk and the iron-free droplets in the FeN<100 approach are similar (e.g. for H_2O_2: 0.56 M s^{-1} and 0.53 M s^{-1}) whereas they are higher into the iron-containing droplets (2.2 M s^{-1}). Since these droplets only comprise 2% of the total LWC, this difference is not reflected in the net uptake rate. At pH = 6 (Fig. S1c and d), the majority of cloud droplets are predicted to be a source of H_2O_2 ~~as the chemical loss rate in the FeBulk droplets and in the iron-free droplets (98% of total) drop by a factor of ~10 between pH = 3 and 6 whereas the source rate slightly increases. This results in a slight supersaturation of~~ ; the only exception are the iron-containing droplets in the FeN<100 approach, from which H_2O_2 evaporates due to less efficient chemical H_2O_2 consumption in the aqueous phase ~~(ϵ ~ 1.05). The reasons for the pH dependence of the ROS concentrations are discussed in detail in (Section 3.2). The~~.

The OH concentrations differ by nearly one order of magnitude between the iron-free and iron-containing cloud droplets (~~e.g., at pH = 4.5:~~ 5.8·10^{-14} M vs 3.3·10^{-13} M, Fig. 2b); the concentration in the FeBulk model is even slightly lower (4.5·10^{-14} M, Fig. 2a). ~~This difference in OH concentrations between the two droplet classes is also reflected in the higher partitioning coefficient ϵ(OH) for the iron-containing droplets as compared to the iron-free droplets and in the FeBulk simulations (b). This trend implies that the gas phase OH concentrations are not significantly different for FeBulk or FeN<100.~~ The reasons for these differences are explored in Section 3.2 where the individual chemical processes affecting the concentrations are analyzed.

~~Partitioning coefficients ϵ for a) H_2O_2, b) OH and c) HO_2 for pH=3 , 4.5 and 6 for FeBulk (filled symbols) and FeN<100 in iron-free (squares) and iron-containing droplets (triangles). Results are shown for simulations of cloud droplets (red) and aerosol particles (blue) at three pH values (3, 4.5, and 6); lines are added to guide the eye.~~

~~The total OH concentration in the cloud water is calculated as a weighted average of the LWCs comprising the iron-free and iron-containing droplets. These concentrations are shown as~~ The bulk aqueous phase ~~concentration at the bottom of b and Fig. S1a,b and c,d, respectively. These concentrations corresponded to those in bulk cloud water samples from cloud droplet populations with $F_{N,Fe}$ = 2% (provided that chemical processes in the sample upon sampling do not change the ROS levels). The total OH concentration~~ OH concentration in the FeBulk approach is approximately 50% higher (4.5·10^{-14} M ~~for FeBulk~~) as compared to 6.4·10^{-14} M for FeN<100 ~~, at pH = 4.5.~~ (Fig. 2). A much greater discrepancy of nearly one order of magnitude between the two approaches is predicted at pH = 6, whereas the difference in the bulk concentrations at pH = 3 is smaller ~~.~~ (Fig. S1). These concentrations corresponded to those in bulk cloud water samples from cloud droplet populations with $F_{N,Fe}$ = 2%, provided that chemical processes in the sample upon sampling do not change the ROS levels (cf also Section 3.3). For all cases, the chemical source and loss rates of the OH radical compensate each other, leading to a relatively small uptake rate of the moderately soluble OH radical into the aqueous phase ($\sim$10^{-16} mol g^{-1} s^{-1}) ~~and~~, which is not significantly affected by ~~the iron distribution ($F_{N,Fe}$).~~

The concentration difference of HO_2/O_2^- between iron-free and iron-containing droplets ~~at pH = 4.5~~ is nearly two orders of magnitude (2.4·10^{-8} M vs 8.9·10^{-10} M) whereas the concentration for FeBulk are predicted ~~in between~~ in-between these two

values (8.9·10⁻⁹ M) ~~. A similar trend is also seen for the ϵ values is between the values for the two drop classes for FeN<100~~
~~(Figs. 3b and 4c~~(Fig. 2). The difference in the concentrations is even greater (~~> factor~~ factor > 200) at pH = 6 (~~Figure~~ Fig. S1d)
whereas they are less than a factor of 3 at pH = 3. These trends suggest that the concentrations are dependent on pH (Section
3.2). The comparison of the bulk aqueous phase HO_2/O_2^- concentrations resulting from the FeN<100 approach (bottom of
Fig. 2b, S2b and d) to those in FeBulk shows that at pH = 4.5 and 6, the total HO_2/O_2^- is underestimated by about one order
of magnitude~~if $F_{N,Fe}$~~ . At pH = ~~2%. The absolute differences between the chemical source and loss rates in the~~ 3, the chemical
loss rate of HO_2/O_2^- in iron-containing droplets is ~~largest (66~~relatively larger than its chemical source rate (74·10⁻⁸ M s⁻¹ vs
~~74~~66·10⁻⁸ M s⁻¹~~) at pH = 3, even though the ratio of these rates is approximately the same at all pH values.~~, Fig. S1b). This
imbalance in the chemical rates leads to a very efficient HO_2 uptake into iron-containing droplets. Consequently, the phase
transfer into these droplets comprises 13% of the total uptake rate ~~(Fig. S1b)~~ whereas at the higher pH values the contributions
correspond to the ratio of LWCs between the two droplets classes (98% : 2%). ~~However, since the effective Henry's law~~
~~constant of HO₂ is relatively small at low pH, HO₂ is nearly at thermodynamic equilibrium ($\epsilon \sim$1, c).~~ The higher Henry's
law constant of HO_2 and rate constants of O_2^- reactions as compared to those of HO_2 at higher pH leads to ~~an increasing~~
~~subsaturation, i.e. to $\epsilon \sim 10^{-3}$ in iron-containing droplets whereas the partitioning of~~ increasingly lower HO_2~~in the iron-free~~
~~droplets and in the FeBulk approach correspond nearly to their equilibrium value (c)~~/O_2^- concentrations with increasing pH.

3.1.2 Aqueous aerosol particles

Since the LWC of the aqueous aerosol particles is smaller by a factor of $2\cdot10^5$ than in clouds, the aqueous phase iron concen-
tration is accordingly higher and so are all chemical rates of iron reactions. Similar to cloud water, the H_2O_2 concentration is
neither significantly affected by the iron distribution nor by iron reactions, i.e., at a given pH value its aqueous phase concen-
tration is nearly the same in all particles. At pH = 4.5 and 6, evaporation of H_2O_2 is predicted for FeBulk and from the iron-free
particles in FeN<100 (Fig. ~~S2c and~~ Fig. 3b and S2b and d). However, since the uptake ~~rate~~ of H_2O_2 into the iron-containing
droplets is much ~~more efficient~~higher, exceeding the evaporation rate by a factor of 25 (-4% vs 104%, ~~b~~pH = 4.5) and $\sim$2
(-143% vs 243% at pH = 6~~, Figure S2d~~), aqueous particles represent a net sink of H_2O_2.

Similar to the cloud case, the OH concentrations in the aqueous phase of FeBulk are between those in the iron-free and iron-
containing particles for FeN<100. The ~~difference between the concentration in iron-free and iron-containing particles is up to~~
~~three orders of magnitude (pH = 3, Figure S2b), which is also reflected in the same difference in ϵ (b). The~~ OH concentrations
do not show a strong pH dependence but their bulk values are about a factor of three lower for the FeN<100 approach ($F_{N,Fe}$ =
2%~~than for $F_{N,Fe}$ = 100%~~) than for the FeBulk approach (1.6·10⁻¹⁵ M vs $\sim$4.6·10⁻¹⁵ M). Even at the high iron concentrations
as present in aerosol water ($\leq$ 0.41 M), the chemical source and loss rates of OH nearly cancel, leading to a relatively small
uptake rate.

The HO_2/O_2^- concentrations in the FeBulk approach are comparable to those as predicted for cloud water at the same
pH value. However, the ~~concentration differences between~~ concentrations in the iron-free and -containing particles ~~are~~differ
~~by~~ four orders of magnitude at pH = 6 (1.5·10⁻⁶ M and 1.3·10⁻¹⁰ M, ~~Figure~~ Fig. S2d). The resulting bulk aqueous phase
concentrations are at least one order of magnitude underestimated by FeBulk (pH = 3); this difference is even a factor of
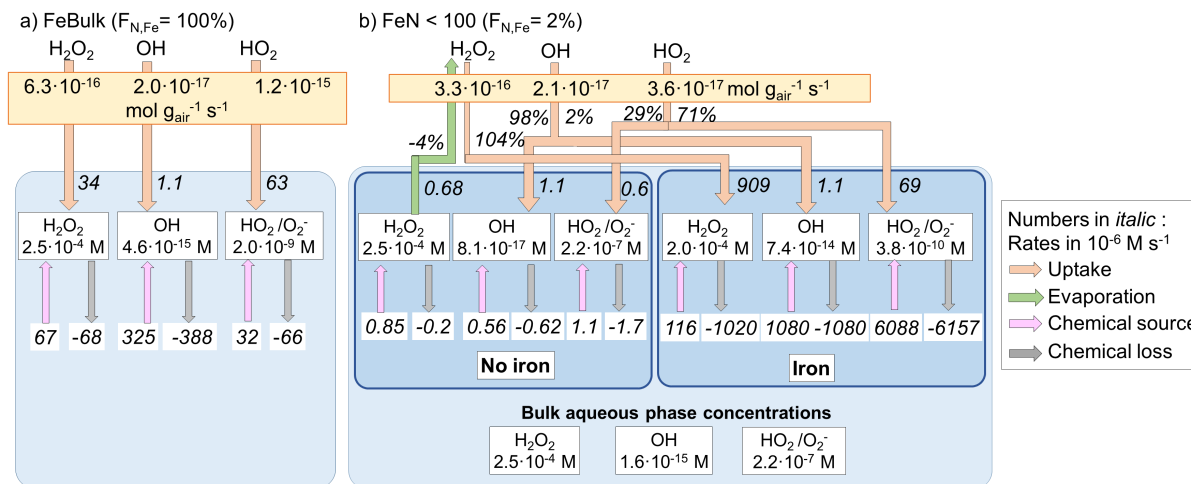
Figure 3. Same as Fig. 2 but for aerosol case (model parameters ~~of the base case~~ in Table 1)

.

2000 at pH = 6 (Figs. 3d and S2d). While the chemical loss rate of HO_2/O_2^- is nearly equal or even larger than ~~the~~ its source rate at pH = 4.5 and 6, ~~respectively,~~ at pH = 3 the source rate exceeds the loss rate resulting in evaporation of HO_2 from the 2% iron-containing particles (Fig. S2b). However, since the uptake rate into the iron-containing particles is larger than this

230   evaporation rate, the net flux of HO_2 is an uptake into the particle phase.

3.2 ~~Relative contributions of chemical reactions and phase transfer to ROS source and loss rates in the aqueous phase~~

~~Generally, a high uptake rate reflects efficient chemical loss and /or inefficient chemical production~~

3.1.1 Gas phase concentrations (OH, HO₂) and mixing ratios (H₂O₂)

235   The gas phase concentrations of OH and HO_2 and mixing ratios of H_2O_2, are shown in Fig. S3 as a function of time (t $\leq$7200 seconds) in the presence of cloud droplets and aerosol particles, respectively, at the three pH values considered here and for the two assumed iron distributions in the aqueous phase. ~~To understand these trends of concentrations~~ The H_2O_2 mixing ratio in the presence of cloud water is very quickly reduced to about 50% of its initial concentration (1 ppb) due to partitioning to the aqueous phase. Both the pH value and $F_{N,Fe}$ have a small effect on the H_2O_2 mixing ratio. The small increase of H_2O_2 over

240   time is in agreement with findings in a recent multiphase box model intercomparison (Barth et al., 2021).

The OH concentrations are on the order of 10^6 cm^{-3}, i.e., typical concentrations as found for continental daytime conditions. This concentrations builds up within a few seconds and does not largely change over the time period considered here. The difference of up to a factor of 5 in the OH concentrations in the presence of cloud droplets with a pH value of 3 and ~~rates as~~

a function of pH as 6, respectively, cannot be directly explained by any OH reactions in the aqueous phase, but are rather a consequence of the OH-HO$_2$ cycle in the multiphase system (Fig. 1). At pH = 6, the effective Henry's law constant for HO$_2$ is highest and therefore, most HO$_2$ is partitioned to the aqueous phase, resulting in the lowest fractions of HO$_2$ in the gas phase. The gas phase HO$_2$ concentrations are on the order of 10^8 cm^{-3}, in agreement with predictions from other atmospheric multiphase chemistry models (e.g., Barth et al. (2021)). Generally, the pH value and iron distributions cause smaller differences in the presence of aerosol particles as compared to the cloud case, since the liquid water content of particles is smaller by several orders of magnitude and therefore a smaller fraction of the species is dissolved.

3.1.2 Partitioning coefficient ϵ

The partitioning coefficient ϵ is often used to describe the distribution of species between the aqueous and gas phases in the atmospheric multiphase system, e.g., Ervens (2015). It is defined as (Fig. 4a). It is defined as

$$\epsilon = \frac{C_{aq}}{p_g \cdot K_{H(eff)}} \tag{4}$$

with C$_{aq}$ and p$_g$ being the aqueous phase concentration [M] and gas phase partial pressure [atm] and $K_{H(eff)}$ the (effective) Henry's law constant [M atm^{-1}]. Accordingly, $\epsilon < 1$ indicates situations when the aqueous phase is subsaturated. Figure 4 summarizes all ϵ values for the cloud and aerosol cases and three pH values.

The ϵ values for the three ROS are summarized in Fig. 4 for the cloud and aerosol simulations at three pH values. The fact that ϵ_{H2O2} is ~1 shows that H$_2$O$_2$ is in thermodynamic equilibrium and explains why its concentrations do not differ among iron-containing and iron-free droplets (particles) (Figs. 2, 3, and S2).

The ϵ_{OH} values in the presence of cloud droplets (red symbols, Fig. 4b) are on the order of ~0.01 - 0.1. The values for iron-containing aerosol particles show a distinct trend with highest ϵ_{OH} values in iron-containing particles, whereas ϵ_{OH} in iron-free particles is lower by two and three orders of magnitude, respectively. The lack of a clear trend in ϵ_{OH} with pH suggests that the main formation and loss processes of OH are pH-independent. The differences in ϵ_{OH} scale with the OH concentrations in aerosol particles that differ by three orders of magnitude between iron-containing and iron-free particles in the FeN<100 approach and the concentration in the FeBulk case (Fig. 3). The ϵ_{OH} values in cloud water do not exhibit such strong differences, which is also reflected in the more similar concentrations in all droplets (Fig. 2). The difference between the concentration in iron-free and iron-containing particles is up to three orders of magnitude (pH = 3, Fig. S2b), which is also reflected in the same difference in ϵ (Fig. 4b).

For the HO$_2$ radical, iron reactions cause a significant deviation from thermodynamic equilibrium at high pH resulting in decreasing ϵ_{HO2} with increasing pH. At high pH, HO$_2$ is more efficiently consumed due to the higher rate constants of the O$_2^-$ radical anion as compared to those with the undissociated HO$_2$ radical. Unlike for OH, for which the smallest ϵ is seen in iron-free particles, the lowest ϵ_{HO2} is found for iron-containing particles - which shows that the concentration differences due to iron distribution for OH and HO$_2$ have different reasons: Whereas iron leads to efficient OH formation, it causes significant HO$_2$/O$_2^-$ loss.
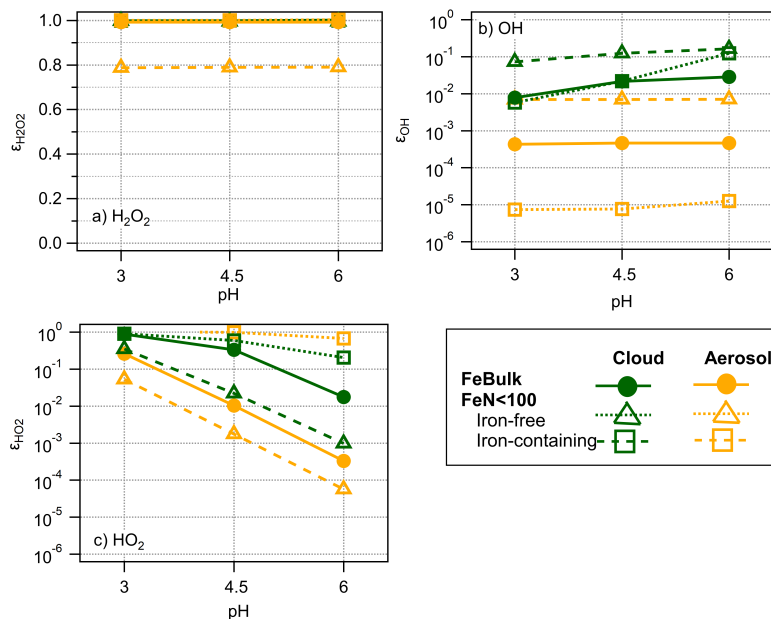
Figure 4. Partitioning coefficients ϵ for a) H_2O_2, b) OH and c) HO_2 for pH = 3 , 4.5 and 6 for FeBulk (filled symbols) and FeN<100 in 98% iron-free (squares) and 2% iron-containing droplets (triangles). Results are shown for simulations of cloud droplets (green) and aerosol particles (orange) at three pH values (3, 4.5, and 6); lines are added to guide the eye.

3.2 Relative contributions of chemical reactions and phase transfer to ROS source and loss rates in the aqueous phase

To understand the trends in concentrations, reaction rates and partitioning coefficients with $F_{N,Fe}$ and pH as discussed in the previous section, Fig. 5 summarizes the main chemical pathways for the three ROS for the cloud and aerosol cases for the same conditions as in Figs. 2 and 3. The individual chemical source (S) and loss (L) processes are indicated between the figure panels for the cloud (top part of figure) and aerosol (bottom part) cases. Only chemical processes are listed that contribute to more than 1% to the ~~corresponding rate for any~~ total rate in each simulation. As the phase transfer (PT) can be a source (i.e., uptake) or loss (i.e., evaporation) process for the aqueous phase species, its contribution is placed between the chemical ~~source and loss contribution. The relative contributions are related to the~~ sources and losses. The total source and loss rates [mol g⁻¹ s⁻¹] ~~as~~ are indicated in the boxes at the upper right in each panel.

Given its high Henry's law constant ($K_{H,H2O2}$ = 1.02·10⁵ M atm⁻¹), the H_2O_2 uptake contributes nearly 50% to the total H_2O_2(aq) source at pH $\leq$ 4.5 in cloud water (Fig. 5a) and even more in aerosol water (50 - 80%) (Fig. 5d). However, ~~as already shown in Figs. 2 and 3,~~ the uptake occurs mostly (98%) into iron-free cloud droplets, whereas in the aerosol case, most H_2O_2 is taken up by the iron-containing particles. This trend was already shown in the comparison of Fig. 2b and 3b. The main loss of H_2O_2 in cloud water is the pH-dependent reaction with sulfur(IV) (L1 in Fig. 5a) whose rate decreases with increasing pH (R4 in Table S1). Therefore, the chemical loss of H_2O_2 in cloud water is very inefficient at pH = 6
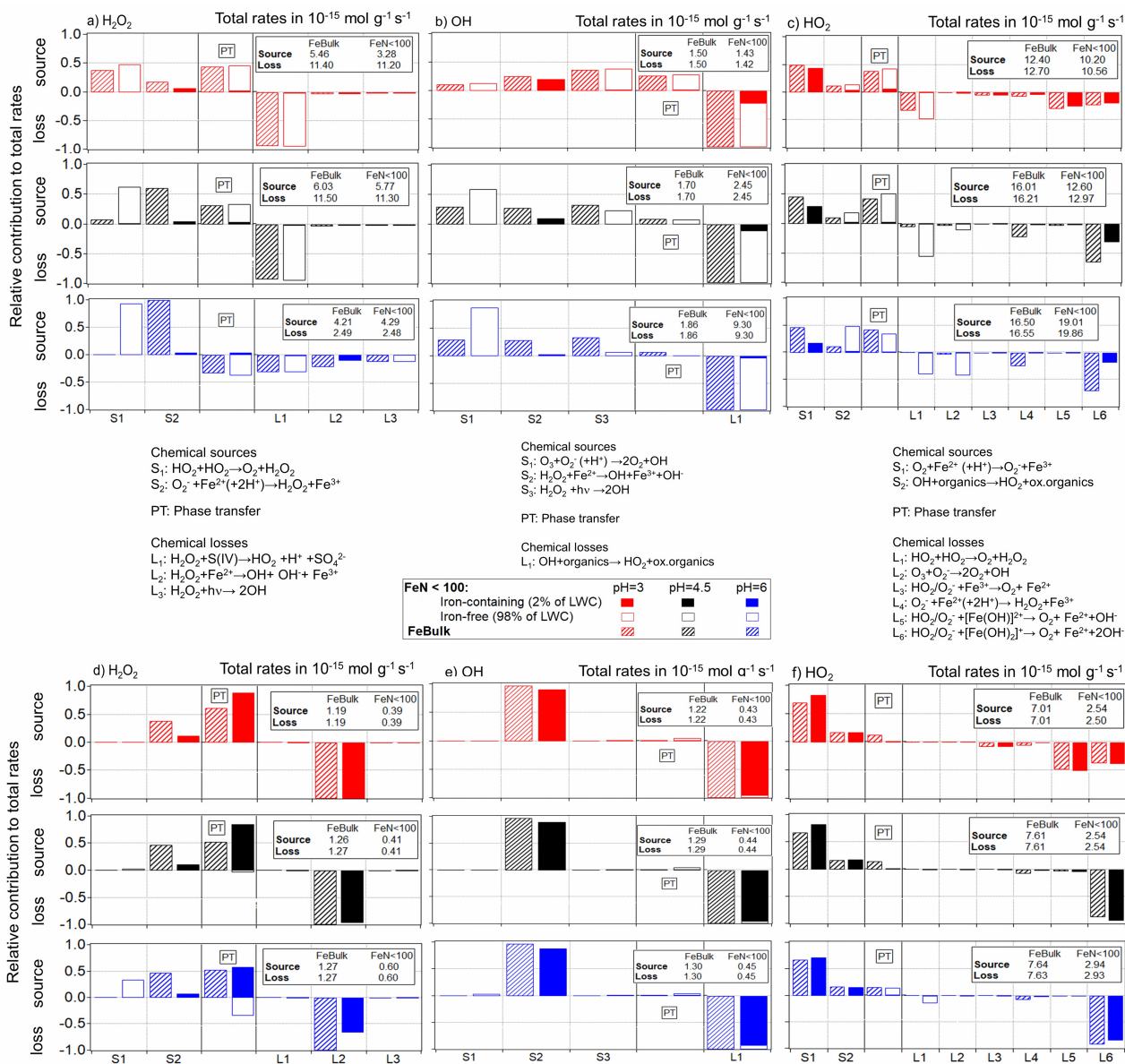
Figure 5. Relative contributions of chemical and phase transfer rates to the total sources and losses of the three ROS. The total rates [mol g_{air}^{-1} s^{-1}] are shown in boxes ~~at the upper right~~ of each panel~~; for~~. For the FeN<100 approach, the contribution in iron-free and iron-containing droplets (particles) are displayed as open and dashed bars; those for the FeBulk approach in solid filled bars. Simulations were performed at constant pH values of pH = 3 (red), 4.5 (black). and 6 (blue) for cloud conditions: a) H_2O_2, b) OH, c) HO_2, and aerosol conditions: d) H_2O_2, e) OH, f) HO_2. The chemical aqueous phase source (S) and loss (L) reactions ~~in the aqueous phase~~ are listed between the panels.

~~in cloud water~~ $2.4\cdot10^{-15}$ mol g^{-1} s^{-1} at pH = 6 vs $\sim11\cdot10^{-15}$ mol g^{-1} s^{-1} at pH $\leq$ 4.5, Fig. 5a). The ~~efficiency of H_2O_2 by~~ rate of the recombination of ~~HO_2~~ H_2O_2 (S1 in Fig. 5a) increases with pH ~~as~~ since the reaction of HO_2 ~~and O_2^-~~ and O_2^- is much faster than with undissociated HO_2 (100·k_{R5} $\sim$ k_{R6}, Table S1). ~~Because of this increasing chemical source and decreasing loss rates with increasing pH, H_2O_2 evaporates from the~~ Therefore, more H_2O_2 is formed at pH = 6 than at lower pH leading to H_2O_2 evaporates from cloud droplets at pH = 6. Figure 5 ~~only~~ represents a snapshot of the rates after a simulation time of 400 seconds. ~~This time corresponds approximately to the lifetime of a single cloud droplet but underestimates the time an aerosol particle might be exposed to a given relative humidity.~~ We have chosen this relatively short time, ~~as in our box model setup, the initialized~~ since gases are not replenished ~~over time~~ during the box model simulations as no emissions are considered. At longer time scales (after 2000 seconds), the conclusions would not be drastically different (Figure ~~S5~~S4); the only major difference is the loss of ~~H_2O_2~~ $_2O_2$ by sulfur(IV) (L1 in Fig. S4a) as SO_2 is consumed quickly within the first few minutes.

In aerosol water, the Fenton reaction (L2, Fig. 5a, d) is the main loss reaction of ~~H_2O_2~~$_2O_2$. The main ~~H_2O_2 source process (S2)~~ $_2O_2$ source process is the reaction of Fe^{2+} with ~~O_2^-~~$_2^-$ (S2) whose rate increases with increasing pH value. Since in iron-free particles, the chemical loss rate (L1) decreases with pH, but its source rate (S1) increases, ~~H_2O_2~~ $_2O_2$ evaporates from iron-free particles. In ~~the~~ iron-containing particles, both the main source and sink reactions are directly dependent on the Fe^{2+} concentration (S2, L2). As the iron concentration in the iron-containing particles is $\sim$50 times higher for FeN<100 than for FeBulk, it seems surprising at first that the chemical rates do not scale by this factor. ~~The HO_2~~Furthermore, the HO_2/~~O_2^-~~$_2^-$ concentration is much higher in iron-free than in iron-containing particles, ~~both in the FeBulk and FeN<100 approach, in~~ in particular at pH = 6. Also this trend, thus, cannot explain the lower chemical ~~H_2O_2~~$_2O_2$ source rates of S2. Therefore, only a difference in the Fe^{2+} concentration can explain the differences in the chemical rates of the chemical ~~H_2O_2~~$_2O_2$ sources and sinks ~~. Indeed, Fe(II)contributes only $\sim$20% to the total iron for $F_{N,Fe}$ = 2% whereas its contribution is $\sim$55% for the FeBulk approach ($F_{N,Fe}$ = 100%) ().~~

~~Predicted Fe(II)/Fe(total) ratios for the a) cloud and b) aerosol cases for pH=3 , 4.5 and 6. Solid lines are for m_{Fe} = 10 ng m^{-3}; dashed lines are for m_{Fe} = 50 ng m^{-3}~~

(Section 4.1).

Independently of the iron distribution, the relative importance of the uptake of the OH radical into cloud water decreases with increasing pH, from $\sim$30% at pH = 3 to < 10% at pH = 6 (Fig. 5b). As the rate of the O_2^- reaction with ozone (S1) increases with pH, the relative importance of this reaction increases with increasing pH value. The loss of OH in the aqueous phase are reactions with organic compounds; the rate of L1 in Fig. 5b and e represents the sum of all reaction rates of OH with organics in Table S1. As the rate constants of OH reactions with carboxylates are generally higher than those with their corresponding acids, the chemical loss rate in cloud water increases with pH. The most striking difference in the source and loss patterns of OH between cloud and aerosol water is the dominating role of the Fenton reaction (S2) as OH source in aerosol water. It contributes nearly 100% of the sources at all pH values, making the OH uptake as a source negligible. Similar to the trends as described above for ~~H_2O_2~~$_2O_2$, the chemical rates of the ~~Fe^{2+}-dependent~~ Fenton reaction as OH source (~~Fenton reaction,~~ S2) is much smaller in ~~for~~FeN<100 than for FeBulk, which can again be explained by the lower Fe(II) concentration at low $F_{N,Fe}$. As the uptake rate of OH is fairly ~~inefficient~~ low as compared to its chemical rates due to its low Henry's low constant ($K_{H,OH}$

= 25 M atm^{-1}, Table S4), the chemical source rate is nearly fully compensated by the chemical loss rate that under all pH and LWC conditions resulting in (nearly) ~~the same value as the source rate~~identical values.

The only major sources of HO$_2$/O$_2^-$ are the reactions of Fe^{2+} with molecular oxygen (S1) and the OH reactions with organics (S2) (Fig. 5c and f). The slight increase in the overall reaction rate of S2 with pH explains the highest chemical source rate in all droplets at highest pH. Its main loss reactions are the reactions of Fe(III) (~~both~~ free Fe^{3+} and the hydroxy complexes [Fe(OH)$_n$]$^{3n-1}$ with n = 1, 2). The dominance of these processes for the loss of HO$_2$/O$_2^-$ leads to very efficient uptake into iron-containing droplets. The rate constants of these loss reactions with ~~the O$_2^-$ radical anion~~ O$_2^-$ are about three orders of magnitude higher than those with ~~the undissociated HO$_2$ radical~~ HO$_2$ (R27, R28, R35-R38 in Table S1). This results in the subsaturation of HO$_2$/O$_2^-$ in the aqueous phase, i.e. decreasing ~~ϵ~~ϵ_{HO2} with increasing pH (Fig. 4c). This effect is more pronounced in aerosol water than in cloud water because of the higher total Fe concentration in particles. The highly efficient loss of O$_2^-$ at high pH results in the lowest HO$_2$/O$_2^-$ concentrations in the iron-containing droplets at pH = 6 (Fig. S2d). Since the reactions of Fe(III) with HO$_2$/O$_2^-$ are the main reduction processes of Fe(III), ~~this low HO$_2$~~the lower HO$_2$/O$_2^-$ concentration leads to inefficient Fe(III) to Fe(II) conversion and relatively higher Fe(III) concentrations ~~. This is reflected in the lower predicted Fe(II)/Fe(total) ratio at low $F_{N,Fe}$ as compared to the FeBulk approach (). The difference in this ratio between $F_{N,Fe}$ = 2% and 100% is about a factor of 2 for cloud water and up to a factor of 3 in aerosol particles. Consequences of this finding for model and field studies are discussed in Section 4.1~~(Section 4.1).

3.3 ~~Difference in aqueous~~ Aqueous phase concentrations ~~and phase transfer rates~~ as a function of $F_{N,Fe}$

3.3.1 ~~Aqueous~~ Comparison of bulk aqueous phase concentrations~~The two~~

The values of $F_{N,Fe}$ = 2% and 100% likely represent extreme values for the iron distribution ~~among cloud droplets or particles~~in cloud droplet or particle populations. While, depending on abundance and proximity of iron emissions sources, also fewer particles (and thus droplets) may contain iron, this would translate into an even higher iron aqueous phase concentration. Under such conditions iron would not be completely dissolved and available for aqueous phase reactions. Therefore, in the following, we limit our discussion to values of $F_{N,Fe} \geq 1\%$. In order to illustrate the total ROS budget in the aqueous phase, Fig. 6 shows the bulk aqueous phase ~~concentration~~concentrations [ROS]$_{aq,bulk}$ [M] calculated based on the LWC-weighted average ROS concentration in the iron-containing and iron-free droplets or particles:

$$[ROS]_{aq,bulk} = [ROS]_{ironfree} \cdot (1 - F_{N,Fe}/100\%) + [ROS]_{iron} \cdot F_{N,Fe}/100\% \tag{5}$$

whereas [ROS]$_{ironfree}$ and [ROS]$_{iron}$ are the ROS concentrations in the iron-free and iron-containing droplets, respectively. (Note that the same calculation was performed for the bulk aqueous phase concentrations in Figs. 2, 3, S1 and S2). Results are shown for the full range of $1\% \leq F_{N,Fe} \leq 100\%$~~and total iron concentrations of 10 ng m^{-3} and 50 ng m^{-3}.

The H$_2$O$_2$ concentrations do not show any dependence on ~~either iron distribution (~~the iron distribution $F_{N,Fe}$ ~~) or iron mass (m_{Fe}) (~~(Fig. 6a and d). ~~As~~ This trend can be explained because (i) in cloud water the main chemical source and loss processes are independent of iron, ~~this finding is obvious. However,~~ whereas (ii) in aerosol water, both the main chemical

source and loss reactions are dependent on the Fe(II) concentration. The same set of processes can also explain why the resulting aqueous phase H_2O_2 concentrations are independent of the total iron mass. In a sensitivity study, we increased m_{Fe}

360   to 50 ng m^{-3} which results in very similar H_2O_2 concentrations (Fig. S5). Thus, a higher iron mass concentration increases both rates by the same factor, resulting in nearly equal H_2O_2 ~~$_2O_2$~~ concentrations for both m_{Fe}.

The OH concentration in cloud water is underestimated by FeBulk by up to a factor of ~ 5 (pH = 6, ~~b); the deviations are only slightly higher for m$_{Fe}$ = 50 ng m^{-3} than for 10 ng m^{-3}~~Fig. 6b). The large difference at the highest pH is the consequence of the more efficient OH formation at pH = 6 by the reaction of O_2^- with O_3 (Section 3.2). Since in the FeN<100 approach the

365   HO_2~~$_2$~~/O_2^-~~$_2$~~ concentration is about one order of magnitude higher at this pH value than for FeBulk, the OH concentration is generally underestimated by assuming $F_{N,Fe}$ = 100%. It can be concluded that in clean conditions, i.e. when the pH value of cloud water is $\geq\sim$5, even for relatively low iron mass concentrations, iron distribution should be taken into account to obtain the correct OH concentrations in cloud water. The deviations are only slightly higher for m_{Fe} = 50 ng m^{-3} than for 10 ng m^{-3} (Fig. S5). In aerosol water, the OH concentration is generally overestimated by FeBulk by factors of $\leq\sim 2$ and ~ 5 for m_{Fe} =

370   10 ng m^{-3} and ~~m$_{Fe}$~~m_{Fe} = 50 ng m^{-3} (~~e~~Fig. 6e and Fig. S5e), respectively. ~~As discussed in the previous section, the~~The lower OH concentration in the FeN<100 approach is a consequence of the lower Fe(II) concentration (~~b~~Section 4.1) which leads to less OH formation by the Fenton reaction.

The HO_2~~$_2$~~/O_2^-~~$_2$~~ concentrations are underestimated in cloud water by the FeBulk approach, approximately by the same factors ($\sim$2 - 5) as the OH radical, with the highest bias at pH = ~~6.~~6 (Fig. 6c). At pH = 3, the difference between the

375   HO_2~~$_2$~~/O_2^-~~$_2$~~ concentrations for the two iron mass concentrations is much larger than for the other pH values. ~~As the total iron concentration in the iron-containing particles is five times higher for the higher~~Unlike for the H_2O_2 and OH concentrations, that are very similar for both m_{Fe}, ~~this leads to even less~~the HO_2/O_2^- concentrations more clearly deviate for the two iron masses considered in Fig. S5. This can be explained by the less efficient Fe(III) reduction ~~(Fe(II)/Fe(total) $\sim$ 0.25 for $F_{N,Fe}$ = 1%,~~ in the cloud droplets at ~~m_{Fe} = 50 ng $^{-3}$) resulting in slightly lower Fe(II)/Fe(total) ratios at~~ at all pH values ~~as compared to~~

380   ~~the lower m_{Fe} (7). With increasing $F_{N,Fe}$ (decreasing iron concentration per particle), the Fe(II)/Fe(total) ratios become similar for both m$_{Fe}$ ($\sim$0.65). The same Fe(II)/Fe(total) ratio at high $F_{N,Fe}$ implies that the Fe(II) concentration scales with m$_{Fe}$ which leads to more efficient HO$_2$/O$_2^-$ loss and lower HO$_2$/O$_2^-$ concentrations at high m$_{Fe}$.~~ Section 4.1).

In aerosol water, the aqueous phase ~~phase~~ ~~concentrations for both m$_{Fe}$ seem~~ HO_2/O_2^- concentrations are nearly identical for wide ranges of $F_{N,Fe}$ ~~. However, the enlarged figure for $F_{N,Fe} \geq$ 60% reveals that the aqueous phase concentrations drop by~~

385   ~~several orders of magnitude with increasing $F_{N,Fe}$ for pH $\geq$ 4.5. Under more acidic conditions (pH~~ at pH = 3 ~~), the difference is much smaller (factor of $\leq$ 10 across the~~ and 4.5, whereas the difference at $F_{N,Fe}$ ~~range~~= 1% and 100% is about one order of magnitude at pH = 6 (Fig. 6f). Thus, the aqueous phase budget of HO_2~~$_2$~~/O_2^- ~~may be underestimated by several orders of magnitude~~ ~~$_2^-$~~ may be significantly underestimated - independently of m_{Fe} - with increasing pH if the iron distribution across the particle distribution is not properly accounted for.

390   ### 3.3.2   ~~Relative difference in phase transfer rates ΔR_{PT}[ROS]~~Enhanced H_2O_2 partitioning into aerosol water, $K_{H,H2O2}$ $= 2.7\cdot10^8$ M atm^{-1}
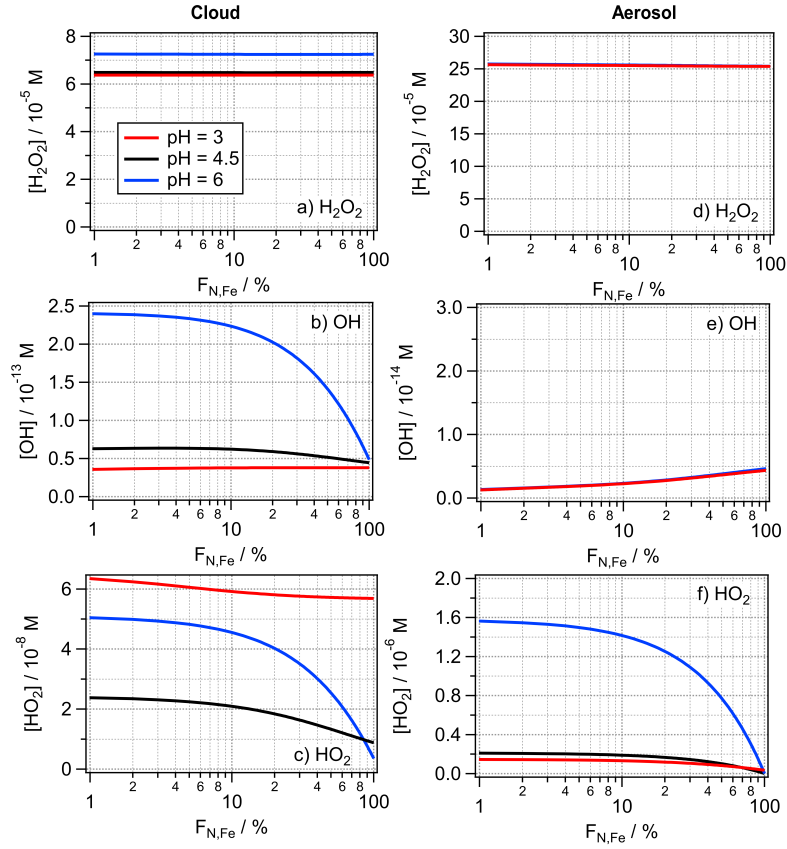
Figure 6. Bulk aqueous phase concentrations of H_2O_2, OH, and HO_2 for the cloud (a - c) and aerosol (d - f) cases as a function of ~~. Solid lines are results for m_{Fe} = 10 ng m^{-3}, dashed lines for m_{Fe} = 50 ng m^{-3}~~ $F_{N,Fe}$ using the model parameters listed in Table 1.

~~As discussed in Sections 3.1 and 3.2, the ROS phase transfer rates are a consequence of an imbalance between the chemical source and loss rates in the aqueous phase. To quantify the differences in the net phase transfer rates, we define~~

$$\Delta R_{PT}[ROS] = \left(\frac{R_{FeN<100}}{R_{FeBulk}} - 1 \right) \cdot 100\%$$ (E.6)

395   ~~whereas R$_{FeN<100}$ and R$_{FeBulk}$ are the net phase transfer rates in the two model approaches. Figure S3 shows ΔR_{PT}[ROS] as a function of $F_{N,Fe}$ for the ROS and cloud and aerosol cases; by definition, ΔR_{PT}[ROS] is zero for $F_{N,Fe}$ = 100%. A positive ΔR_{PT}[ROS] mans that the phase transfer rate is underestimated by the FeBulk approach.~~

~~Similar to the differences in ROS aqueous phase concentrations in , large differences in H_2O_2 phase transfer rates are predicted for cloud droplets at pH = 6 because of the inefficient H_2O_2 consumption in iron-free droplets. In aerosol water,~~
400   ~~the phase transfer rates of H_2O_2 differ by up to a factor of ~2 (ΔR_{PT}[H_2O_2] $\geq$ -100%). However, since the H_2O_2 uptake is sufficiently efficient to maintain thermodynamic equilibrium, such differences in H_2O_2 uptake rates may be negligible.~~

For the OH radical, the highest discrepancy between the uptake rates is predicted at pH = 4.5 ($\leq$ 30 - 50%, depending on m_{Fe}, Figure S3b). For FeBulk, the OH concentration in clouds is nearly independent of pH ($3.9 \cdot 10^{-14}$ M $\leq$ OH $\leq 4.5 \cdot 10^{-14}$ M, Figs. 2 and S2). However, for FeN<100, the OH concentration is increasing with pH in the iron-free droplets whereas it is slightly decreasing in the iron-containing droplets. These opposite trends are due to the non-linear rate of the HO_2/O_2^- recombination, that is highest at pH = 4.5 and dominating OH formation in the iron-free droplets whereas in the iron-containing droplets the pH-independent Fenton reaction is the most important OH source (b). In aerosol, ΔR_{PT}[OH] are even smaller, on the order of < 5%, even though OH is not in thermodynamic equilibrium ($\epsilon < 1$, b).

The relative differences in HO_2 for m_{Fe} = 10 ng m^{-3} are < 20% for all conditions in cloud water (Fig. S3c). The highest value is predicted at pH = 3 and m_{Fe} = 50 ng m^{-3} as a consequence of the increasing difference of the HO_2 formation rate by the Fe(II) reaction with molecular oxygen and its loss rate via its reaction with Fe(III) (c) and the low Fe(II)/Fe(total) ratio. For the aerosol case, the phase transfer rates of HO_2 differ by up to a factor of ~2 (ΔR_{PT}[HO$_2$] $\geq$ -100%), depending on $F_{N,Fe}$, with the smallest deviation at pH = 6 (ΔR_{PT}[HO$_2$] $\geq$ -60%). At high pH, the phase transfer is relatively more important as HO_2 source ($\leq$ 20%) as compared to the more acidic conditions (f). The evaporation of HO_2 at pH = 3 from the iron-free particles reduces the net uptake rate of HO_2 into the particle phase. Therefore, the difference in the net uptake rates are largest at low pH value.

The uptake of OH and HO_2 into aerosol particles is often parameterized by the dimensionless reactive uptake coefficient γ (Thornton and Abbatt, 2005; Mao et al., 2013, 2017) that is derived based on the first-order radical loss (k^{loss}) onto aerosol particles:

$$k^{loss} = \gamma \frac{\omega S}{4} \tag{E.7}$$

with ω being the molecular speed,

$$\omega = \sqrt{\frac{8RT}{\pi M}} \tag{E.8}$$

whereas M is the molar mass g mol^{-1}, R is the gas constant, and T is the absolute temperature K, and S the aerosol surface, e.g., Thornton and Abbatt (2005); Pöschl et al. (2007). Accordingly the phase transfer rate of the radicals into the particle phase can be described as

$$\frac{d[Radical]_g}{dt} = k^{loss}[Radical]_g \tag{E.9}$$

corresponds to the first right-hand term of and thus, γ values for OH and HO_2 were derived based on the phase transfer rates in Figure S3 (). We do not show values for H_2O_2 since its partitioning can be described based on Henry's law.

The γ values for HO_2 into cloud water are in the range of 10^{-3} - 10^{-2} with higher values at the highest pH. The weak $F_{N,Fe}$ dependence of the total phase transfer rates into cloud water (Fig. S3c) is also reflected in its γ values with the highest value at pH = 6, when also the phase transfer rate is highest. The γ(OH) values show even less difference between different pH values

~~and $F_{N,Fe}$ (note the linear scale in a). Thus, the reactive uptake of OH into cloud droplets could be parameterized by a constant value of $\gamma \sim 6\cdot10^{-3}$ for all conditions explored here.~~

~~Reactive uptake coefficients $\gamma(OH)$ and $\gamma(HO_2)$ derived from the multiphase model studies at three pH values for a, b) cloud,~~
435 ~~c, d) aerosol conditions. The solid and dashed lines show results for m_{Fe} = 10 and 50 ng m^{-3}, respectively.~~

~~In aerosol water, $\gamma(HO_2)$ shows a strong dependence on $F_{N,Fe}$, leading to an overestimate of the reactive uptake by FeBulk by up to two orders of magnitude at pH = 3 (c). Note that at $F_{N,Fe}$ = 1% no γ value is shown as under such conditions, HO$_2$ is predicted to evaporate. This evaporation is due to the inefficient HO$_2$ consumption in iron-free particles but efficient uptake into the iron-containing particles, independent of the aqueous phase concentration. This leads to a great imbalance of the phase~~
440 ~~transfer rates from and into the two droplet classes than shown in b. Similar to the findings for cloud water, the uptake of the OH radical could be parameterized by a single γ value for the conditions applied here ($\gamma \sim 0.0045$).~~

3.3.3 ~~Enhanced~~

Strictly, Henry's law constants are not applicable to highly concentrated aqueous solutions such as aerosol water. Simultaneous measurements of particle-bound and gas phase ~~H$_2$O$_2$~~ O_2 concentrations suggest that it partitions much more efficiently to
445 the particle phase than predicted based on its physical Henry's law constant (~~K$_{H,H2O2}$~~ $K_{H,H2O2}$ = 1.02$\cdot10^5$ M atm^{-1}). Despite large uncertainties in such measurements and of related parameters such as the aerosol water content, various studies revealed that the partitioning of ~~H$_2$O$_2$~~ O_2 between the gas and the aerosol aqueous phases may be more appropriately described with an effective Henry's law constant of ~~K$_{H,eff,H2O2}$~~ $K_{H,H2O2} \leq 2.7\cdot10^8$ M atm^{-1} (Hasson and Paulson, 2003; Xuan et al., 2020). The observation by Hasson and Paulson (2003) of higher ~~H$_2$O$_2$~~ O_2 concentrations in coarse mode particles than in fine mode
450 particles might point to a size-dependent chemical particle composition with higher iron content in coarse particles that often contain dust.

To explore the effects of such enhanced partitioning, we performed a sensitivity study, using ~~K$_{H,eff,H2O2}$~~ $K_{H,H2O2} \leq 2.7\cdot10^8$ M atm^{-1}. In ~~Figure S4~~ Fig. S6, the aqueous phase concentrations and net phase transfer rates of the three ROS are compared to those using the physical Henry's law constant (~~K$_H$(H$_2$O$_2$)~~ $K_{H,H2O2}$ = 1.02$\cdot10^5$ M atm^{-1}). No other parameter was changed as
455 to our knowledge corresponding ~~K$_{H,eff}$~~ $K_{H(eff)}$ for OH and/or ~~HO$_2$~~ $_2$ are not available. We perform this comparison only for the aerosol case, as numerous measurements have shown that the partitioning of ~~H$_2$O$_2$~~ O_2 into cloud water can be satisfactorily described by its ~~K$_H$~~ K_H (e.g., Ervens (2015)).

As expected, a higher (~~K$_{H,eff,H2O2}$~~ $K_{H,H2O2}$) results in higher ~~H$_2$O$_2$~~ O_2 aqueous phase concentrations by three orders of magnitude. ~~Also the phase transfer of H$_2$O$_2$ into the particle phase is more efficient even though the difference in the rates is~~
460 ~~smaller than the ratio of the K$_{H(eff)}$ values. However, unlike~~ Unlike for the low ~~K$_{H,H2O2}$~~ $K_{H,H2O2}$, the higher partitioning leads to smaller ~~H$_2$O$_2$~~ O_2 concentrations for FeBulk than for FeN<100 by up to one order of magnitude and pH = 6. The OH concentration in the aqueous phase is predicted to decrease with increasing $F_{N,Fe}$, unlike in ~~our~~ the base case simulation where we showed the opposite trend (Fig. ~~S4b~~ S6b). The higher ~~H$_2$O$_2$~~ O_2 concentration generally increases the importance of the Fenton reaction and photolysis ~~leading to more~~ for OH production in the aqueous phase. While the ~~HO$_2$~~ $_2$/O$_2^-$ concentrations
465 for the two ~~K$_{H,H2O2}$~~ $K_{H,H2O2}$ values do not differ at low $F_{N,Fe}$, they are significantly smaller by several orders of magnitude for

the higher $K_{H,H2O2}$ (Figure S4c). For the full range of $F_{N,Fe}$, the Fe(II)/Fe(total ratio does not exceed ~20% (Fig. S4g). Thus, HO₂/O₂⁻ is always efficiently consumed by Fe(III). This predicted independence of Fe(II)/Fe(total) ratio as a function of $F_{N,Fe}$ for the high $K_{H,eff,H2O2}$ in contrast to the predicted strong dependence by using the physical $K_{H,H2O2}$ may be used to guide future experiments to determine the 'best' value of $K_{H,eff,H2O2}$ for aerosol water. $K_{H,H2O2}$ (Fig. S6c).

470 The predicted phase transfer rates for OH and HO₂ are nearly the same for both $K_{H(eff),H2O2}$ at $F_{N,Fe} > \sim 10\%$ which implies that the derived γ values for these radicals might apply for both $K_{H(eff),H2O2}$ values. However, at $F_{N,Fe} < 10\%$, we predict a net evaporation of HO₂ from the particle phase ($R_{PT}HO_2 < 0$, Fig. S4f). This implies that the particle phase is supersaturated in HO₂/O₂⁻. Such considerations need to be taken into account in studies of the ROS formation potential of particles in the context of oxidative properties and health effects of particulate matter, e.g. (Saffari et al., 2014; Tong et al., 2016, 2020) (Section 4.3).

4 Implications of $F_{N,Fe} < 100\%$ for model and field studies

4.1 Oxidation state of iron: Fe(II)/Fe(~~III~~total)

The iron oxidation state determines its solubility and bioavailability since Fe(II) salts are usually more soluble than Fe(III) compounds. Fe(II) usually dominates during daytime because Fe(III) complexes are readily photolysed (Deguillaume et al., 2005). Reported measurements are based on analyses that are performed on bulk samples where redox reactions of iron can occur af-

480 ter collection and combination of all cloud droplets or aerosol particles, respectively. The trends and overall Fe(II)/Fe(~~III~~total) (or Fe(II)/Fe(III)) ratios have been reproduced in several model studies that all assumed that iron is present in the complete aqueous phase (Ervens et al., 2003; Deguillaume et al., 2004; Luo et al., 2005; Tilgner et al., 2013; Ingall et al., 2018). Thus, the agreement between measured and predicted data is not surprising as both types of studies imply that the total soluble iron is evenly distributed throughout the total aqueous volume.

485 However, our study reveals that these Fe(II)/Fe(~~III~~total) ratios are not the true ratios present in the atmospheric aqueous phases if iron is only present in a small number fraction of particles or droplets. In cloud water, the soluble iron fraction (~Fe(II)/Fe(total)) might be overestimated by up to factor of 2 (Fig. 7a) whereas this bias might be even higher in aerosol particles (≤~2.5 (Fig. 7b). The overview articles by Deguillaume et al. (2005) and Mao et al. (2017) show large ranges of the Fe(II)/Fe(total) fraction (10 - 100%). Interestingly the study by Takahama et al. (2008) that investigated single particles

490 report values at the lower end of this range (~20%). We cannot state with certainly that this finding is due to different aerosol composition or origin or indeed points to a more accurate representation of the Fe(II)/Fe(~~II~~total) ratio in individual particles rather than in bulk samples.

If the Fe(II))/Fe(total) may be considered a measure of the bioavailability of iron, it might be actually lower than derived from ambient samples or model studies, if they apply a bulk approach. Our results suggest that parameterizations of the

495 Fe(II)/Fe(total) ratios as, for example suggested by (Mao et al., 2017), might have to be further refined to account for the effects due to the iron distribution across particle populations. In aqueous media that consist of a bulk aqueous phase (e.g., oceans, lung fluid, to some extent also rain water), the Fe(II) fraction will be appropriately represented by FeBulk ($F_{N,Fe} = 100\%$ (FeBulk). The time scales for the Fe(II)/Fe(III) ratio to adjust from conditions of $F_{N,Fe} < 100\%$ to $F_{N,Fe} = 100\%$ will
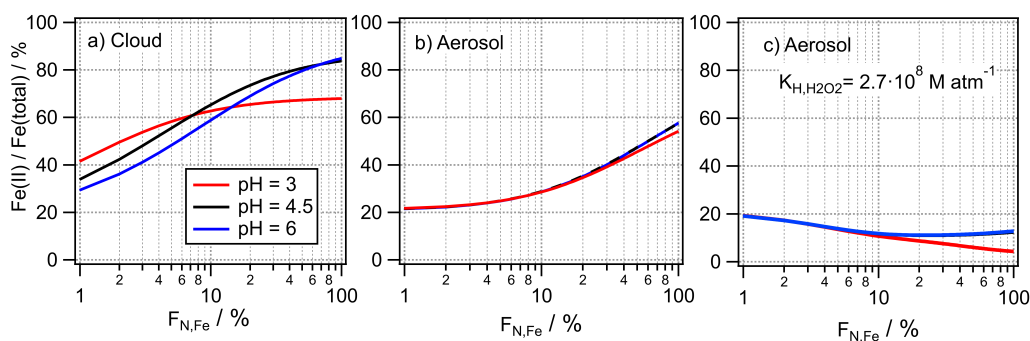
Figure 7. Predicted Fe(II)/Fe(total) ratios at pH = 3 , 4.5 and 6 and the conditions as given in Table 1. a) Cloud, b) Aerosol, c) Aerosol with enhanced partitioning of H_2O_2 ($K_{H,H2O2}$ = 2.7·10^8 M atm^{-1}; Section 3.3.3).

depend on the rates of iron redox processes, and on the solubility and dissolution kinetics of ferrous and ferric salts ~~which in~~
500 ~~turn maybe~~ , which, in turn, may be a function of other solutes and liquid water content. If H_2O_2 is more soluble in aerosol water than in cloud water ($K_{H,H2O2}$ = 2.7·10$_8$ M atm^{-1}; Section 3.3.3), the Fe(II)/Fe(total) ratio does not exceed ∼20% for any $F_{N,Fe}$ (Fig. 7c). Thus, HO_2/O_2^- is always efficiently consumed by Fe(III), even at the highest considered iron mass (50 ng m^{-3}, Fig. S7c). This predicted independence of Fe(II)/Fe(total) ratio as a function of $F_{N,Fe}$ for the high $K_{H,eff,H2O2}$ in contrast to the predicted strong dependence by using the physical $K_{H,H2O2}$ may be used to guide future experiments to determine the 'best'
505 value of $K_{H,eff,H2O2}$ for aerosol water.

4.2   ~~Application of reactive~~ Reactive uptake parameters ~~g~~γ

4.2.1   ~~Reactive uptake coefficient~~ Calculation of ~~the hydroxy radical, γ(OH)~~γ_{OH} and γ_{HO2}

The ~~values for~~ uptake of OH and HO_2 into aerosol particles is often parameterized by the dimensionless reactive uptake coefficient γ ~~(OH) derived based on our model studiesfor both iron mass concentration and~~ that is derived as a function of the
510 first-order radical loss (k^{loss}) onto aerosol particles. For the derivation of γ based on lab studies, it is assumed that γ solely depends on the molecular speed and the droplet surface. However, it has been discussed that the reactive uptake coefficient in atmospheric applications should also include a term to account for gas phase diffusion ((Jacob, 2000)):

$$k^{loss} = \left(\frac{r_d}{D_g} + \frac{4}{\omega \gamma} \right)^{-1} S \tag{7}$$

with S being the total droplet surface area per air volume and ω the molecular speed,

515 $$\omega = \sqrt{\frac{8RT}{\pi M}} \tag{8}$$

whereas M is the molar mass [g mol^{-1}], R is the gas constant, and T is the absolute temperature [K] (e.g., Thornton and Abbatt (2005); Pösch). Accordingly, the phase transfer rate of radicals into the particle phase can be described as

$$\frac{d[Radical]_g}{dt} = k^{\text{loss}}[Radical]_g \tag{9}$$

and the reactive uptake coefficient γ can be derived as

520 $$\gamma = \frac{4}{\omega\left(\frac{S}{k^{\text{loss}}} - \frac{r_d}{D_g}\right)} \tag{10}$$

The γ values for OH and HO$_2$ as a function of Fe_{NFe} are displayed in Fig. 8. If gas phase diffusion is neglected in the derivation of γ, the last term in the denominator of Equation 10 is set to zero (Equation S.3). To demonstrate the impact of gas phase diffusion on the reactive uptake parameter, we compare γ values calculated with Equation 10 to values without consideration of gas phase diffusion (Section S3 in the Supplement).
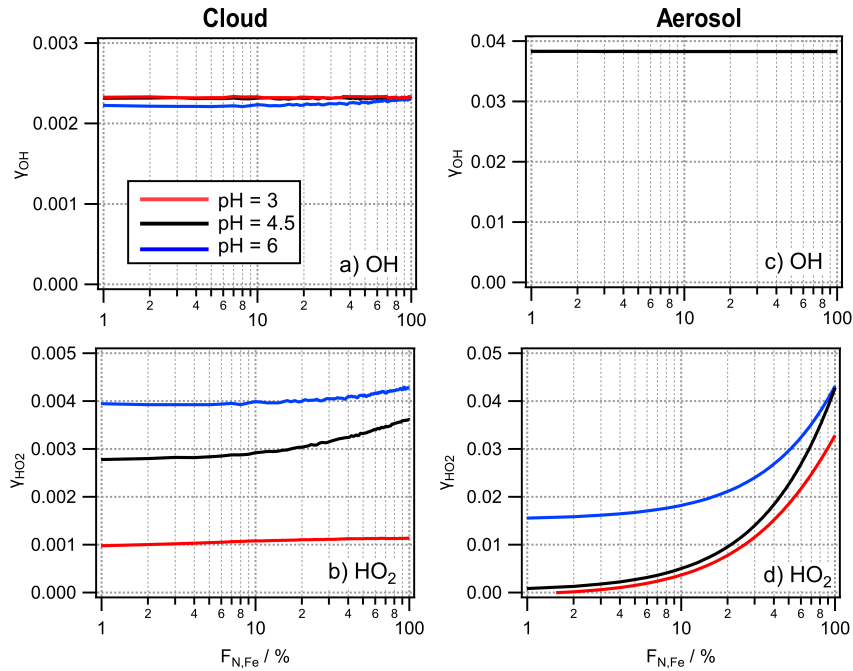
Figure 8. Reactive uptake coefficients γ_{OH} and γ_{HO2} derived from the multiphase model studies at three pH values for a, b) cloud, c, d) aerosol conditions.

525 **4.2.2 Reactive uptake coefficient of the hydroxy radical, γ_{OH}**

The derived values for γ_{OH} over the full range of $F_{N,Fe}$ (~~5.8~~2.2·10⁻³ $\leq$ ~~γ(OH) cloud~~ γ_{OH}(cloud) $\leq 6.4\cdot10^{-3}$; ~~γ(OH) aerosol~~ γ_{OH}(aerosol) $\sim$ ~~4.5~~3.8·10~~⁻³~~⁻² are in good agreement with the average value suggested for pure water surfaces (~~γ~~ γ_{OH} = 0.035) (Hanson et al., 1992). It should be noted that this latter experimental value was derived assuming a Henry's law constant of ~~K_H(OH)~~ $K_{H,OH} \geq 40$ ~~atm M~~ M atm⁻¹ and [OH] $\geq 10^8$ cm⁻³. If it were adjusted to atmospherically more relevant conditions ([OH] $\sim 10^6$ cm⁻³) and ~~the K_H(OH)~~ $K_{H,OH}$ = 25 M atm⁻¹ as used in our study (Table S4), the resulting ~~γ(OH)~~ γ_{OH} might be smaller by more than order of magnitude than the reported one. Molecular dynamics simulations for the mass accommodation of OH on water surfaces showed ~~α(OH)~~ α_{OH} = 0.1 which can be considered the upper limit of reactive OH uptake onto water surfaces (Roeselová et al., 2003). The difference between such a value for pure water and the values from our model study demonstrate the high reactivity of the OH radical in the aqueous phase. As its solubility is limited, this high reactivity results in subsaturated conditions (~~ε(OH)~~ ϵ_{OH} < 1; Fig. 4b). The γ_{OH} values show little difference at different pH values and $F_{N,Fe}$. Thus, the reactive uptake of OH into cloud droplets could be parameterized with a value of $\gamma_{OH} \sim 2.3\cdot10^{-3}$ for all conditions explored here. Similar to the findings for cloud water, the uptake of the OH radical could be parameterized by a single γ value for the conditions applied here ($\gamma_{OH} \sim 0.0038$). The comparison of the values in Fig. 8a and c to those in Fig. S8a and c reveals that the gas phase diffusion leads to a significant decrease of γ_{OH} by a factor of $\sim$3 in clouds and $\sim$ 10% in aerosol particles.

Several previous studies have determined ~~γ(OH)~~ γ_{OH} on surfaces other than pure water that are more comparable to atmospheric aerosol particles. Hanson et al. (1992) showed that ~~γ(OH) increases in~~ γ_{OH} increases on acidic solutions from 0.07 (28% H₂SO₄) to unity ~~in~~ on 96% H₂SO₄. On organic surfaces, ~~γ(OH~~γ_{OH}) values are generally higher than on inorganic surfaces which demonstrates the high reactivity of OH with organics in the condensed phase and/or on organic surfaces. In several lab studies, squalane was used as a proxy for long-chain ~~alkane~~alkanes; the reactive uptake coefficients have been determined in a range of $\sim$0.2 < ~~γ(OH)~~ γ_{OH} < 0.5 (e.g., ~~Che et al. (2009); Smith et al. (2009); Waring et al. (2011); Houle et al. (2015); Bianchini et al. (~~ (Che et al., 2009; Smith et al., 2009; Waring et al., 2011; Houle et al., 2015; Bianchini et al., 2018; Li and Knopf, 2021)). A similar value range was also found for a wide variety of other organics (~~(Bertram et al., 2001)~~Bertram et al. (2001)). In other experimental studies on organic particles, ~~γ(OH)~~ γ_{OH} > 1 were found (~~γ(OH)~~ γ_{OH} = 1.64 on wet succinic acid (Chan et al., 2014), 1.3 $\pm$ 0.4 on bis(2-ethylhexyl) sebacate (George et al., 2007)). ~~γ(OH)~~ γ_{OH} on organic aerosols may decrease with increasing OH gas phase concentration because the viscosity of the organic condensed phase prevents efficient uptake and diffusion of OH towards the particle center (Slade and Knopf, 2013; Arangio et al., 2015). Such effects were included in recently developed frameworks to parameterize ~~γ(OH)~~ γ_{OH} as a function of particle viscosity, size and gas phase OH concentration (Renbaum and Smith, 2011; Houle et al., 2015).

We did not explore any of these parameters in detail in our current model study. However, the comparison of the tight range of our ~~γ(OH)~~ γ_{OH} values in Fig. 8, independently of $F_{N,Fe}$ and cloud or aerosol aqueous conditions, to the wide ranges of literature values, leads us to the following conclusions: (i) The similarity of our ~~γ~~ γ_{OH} value based on an explicit chemical mechanism to that measured on pure water suggests that $\sim10^{-3}$ < ~~γ(OH)~~ $\gamma_{OH} \sim 10^{-2}$ may be a good approximation ~~for~~ under cloud conditions. (ii) The fact that we cannot reproduce the high ~~γ(OH)~~ γ_{OH} values as observed on organic aerosols suggests that organic reactions control the reactive uptake of OH which are not included in our explicit chemistry scheme. (iii) Since

560 organics are likely present in all aerosol particles, the effect of the iron distribution ($F_{N,Fe}$) for $\gamma(OH)$ γ_{OH} may be overestimated by our chemical mechanism on ambient aerosol particles.

4.2.3 Reactive uptake coefficient of the hydroxy peroxyl radical, $\gamma(HO_2)$ γ_{HO2}

The γ_{HO2} values into cloud water are in the range of 0.001 - 0.004 with higher values at the highest pH (Fig. 8b). In aerosol water, γ_{HO2} shows a strong dependence on $F_{N,Fe}$, leading to an overestimate of the reactive uptake by FeBulk by up to two

565 orders of magnitude at pH = 3 (Fig. 8d). Note that at $F_{N,Fe}$ = 1%, no γ_{HO2} value is shown as under such conditions, HO$_2$ is predicted to evaporate. This evaporation is due to the inefficient chemical HO$_2$ consumption in iron-free particles, whereas efficient uptake occurs into the iron-containing particles. This leads to a great imbalance of the phase transfer rates from and into the two droplet classes as shown in Fig. 2b. We use identical α values for droplet and aqueous particle surfaces. The mass accommodation coefficient α is the upper limit of the maximum value for the uptake coefficient γ. This limit can be seen in

570 Equation 10d where γ_{HO2} approaches the value of α_{HO2} = 0.05, i.e., the regime, at which the uptake is fully controlled by the mass accommodation and not by the chemical loss in the aqueous phase. For the HO$_2$ radical, gas phase diffusion may decrease γ_{HO2} by a factor of $\sim$2 at pH = 6 whereas the two two γ values are nearly identical at pH = 3 (Fig. S8b). In aerosol water, gas phase diffusion has an insignificant impact on its reactive uptake coefficient onto aerosol water (Fig. S8d).

It has been shown in global model studies, that the the reactive loss of HO$_2$ $_2$ on aerosol surfaces can significantly impact the

575 atmospheric oxidant budget, e.g. ~~(Haggerstone et al., 2005; Macintyre and Evans, 2011; Stadtler et al., 2018; Li et al., 2019)~~ Haggerstone et al. (2005); Macintyre and Evans (2011); Stadtler et al. (2018); Li et al. (2019). A value of $\gamma(HO_2)$ γ_{HO2} = 0.2 based on the study by Jacob (2000) has been commonly used in global models, which has also been supported by molecular dynamics simulations (Morita et al., 2004). However, recent model studies ~~suggested~~ suggest that this value may be an overestimate and that values on the order of $\gamma(HO_2)$ γ_{HO2} = 0.05 or 0.08 may be more appropriate (Christian et al., 2017; Tan et al.,

580 2020).

On dry aerosol surfaces, $\gamma(HO_2)$ γ_{HO2} is usually low: For example, Bedjanian et al. (2005) measured $\gamma(HO_2)$ γ_{HO2} = 0.075 $\pm$ 0.015 on dry soot surfaces which is comparable to the value of $\gamma(HO_2)$ γ_{HO2} $\leq$ 0.031 on dust (Matthews et al., 2014) and γ γ_{HO2} < 0.01 on dry NaCl (Remorov et al., 2002). $\gamma(HO_2)$ γ_{HO2} increases by more than one order of magnitude when RH increases from $\sim$20% to > 90% (Cooper and Abbatt, 1996; Taketani et al., 2008; Lakey et al., 2015, 2016; Moon et al., 2018).

585 Lakey et al. (2015) showed much higher $\gamma(HO_2)$ γ_{HO2} values on two humic acids (0.0007 ~~$\leq$ $\gamma(HO_2)$ $\leq$~~ $\leq$ γ_{HO2} $\leq$ 0.06 and 0.043 $\leq \gamma_{HO2}$) $\leq$ 0.09, respectively) than on pure long-chain carboxylic acids ($\gamma(HO_2)$ γ_{HO2} < 0.004). They ascribed the higher HO$_2$ $_2$ uptake to the small concentrations of copper and iron ions in the humic acids, in agreement with previous studies that showed the large impact of TMI ions on HO$_2$ reactive uptake (e.g., ~~(Mao et al., 2013, 2017)~~ Mao et al. (2013, 2017)). It was suggested by ~~(Lakey et al., 2015)~~ Lakey et al. (2015) that the HO$_2$ uptake cannot be solely controlled by the TMI ion

590 concentration as they did not see any correlation with $\gamma(HO_2)$ γ_{HO2}. This lack of trend is similar to findings by Mozurkewich et al. (1987) who also did not find any clear relationship in $\gamma(HO_2)$ γ_{HO2} on Cu-doped NH$_4$HSO$_4$ and LiNO$_3$ particles with Cu concentration.

Based on our model results, the lack of such correlation can be qualitatively understood by simultaneous increase of the main chemical HO$_2$ source and sink rates (Reactions S1 and L4- L6 in Fig. 5f). The absence of a dependence of HO$_2$ uptake

595 on wet particle diameter in the study by Mozurkewich et al. (1987) is also in agreement with our sensitivity studies in which we varied the particle diameter by a factor of ± 2 (Fig. ~~S6~~S9). This implies that the interfacial mass transfer is not a limiting step in the HO$_2$ uptake. The HO$_2$ uptake on Cu-doped ammonium sulfate particles was observed to be higher under neutral (~~γ(HO$_2$)~~ γ_{HO2} = 0.2) as opposed to acidic conditions (~~γ(HO$_2$)~~ γ_{HO2} = 0.05) (Thornton and Abbatt, 2005). Similar results were ~~also~~ observed by Mao et al. (2013) who generally found somewhat higher values than in our study (~~γ(HO$_2$)~~ γ_{HO2} > 0.4)

600 and highest values for lowest Cu/Fe ratios (i.e., highest iron concentration at a constant copper concentration) and highest pH. However, overall their differences in ~~γ(HO$_2$)~~ γ_{HO2} due to Fe/Cu ratio and/or pH are smaller than those that we predict for different $F_{N,Fe}$ ($\sim 10^{-4}$ ≤ ~~γ(HO$_2$)~~ ≤ γ_{HO2} ≤ $\sim 10^{-2}$, at pH = 3). This suggests that ~~γ(HO$_2$)~~ γ_{HO2} parameterizations that take into account the dependence on Cu concentration, total aerosol mass and particle size, e.g., ~~Guo et al. (2019); Song et al. (2020)~~ (Guo et al., 2019; Song et al., 2020), should be further refined to also include the iron distribution.

605 We note that our results are not quantitatively comparable to those on Cu-doped particles as our chemical scheme includes only reaction of iron as the only TMI. The corresponding reactions with Cu$^{+/2+}$ have generally higher rate constants than those of iron reactions (Ervens et al., 2003; Deguillaume et al., 2004); however, as copper concentrations in ambient aerosols are usually lower than iron concentrations, the effect of both TMIs might be similar. We did not perform the equivalent simulations for copper in the present study as to our knowledge, there is no data available that give single-particle information on the

610 distribution of iron and copper within droplet or particle populations. However, if iron and copper originated from different emission sources, the number concentration of TMI-containing particles might be relatively high. However, in such situations the synergistic effects of Fe and Cu affecting HO$_x$ cycling and uptake as suggested by (Mao et al., 2013) might be reduced.

Measurements of ~~γ(HO$_2$)~~ γ_{HO2} on ambient aerosol populations showed ranges of 0.13 ≤ ~~γ(HO$_2$)~~ ≤ γ_{HO2} ≤ 0.34 (Mt. Tai) and 0.09 ≤ ~~γ(HO$_2$)~~ ≤ ≤ γ_{HO2} ≤ 0.4 (Mt. Mang) ~~Taketani et al. (2012)~~ (Taketani et al., 2012). No systematic trend with total

615 iron concentration that exceeded 1 μg m^{-3} at Mt Mang and 10 μg m^{-3} at Mt Tai was observed. The acidity of the aerosols was not reported in that study; however, the derived ~~γ(HO$_2$)~~ γ_{HO2} values did not show any significant trend with the molar NH$_4^+$/(SO$_4^{2-}$ + NO$_3^-$) ratios that ranged from ~ 1 - ~ 2 and ~ 2 - ~ 3, pointing to moderately acidic to fully neutralized aerosol. The fact that the ambient data do not show any trend with acidity might either point to a high number fraction of TMI-containing particles and/or to a relatively high pH, i.e. to conditions under which our model results do not show a large effect of $F_{N,Fe}$

620 (Fig. 8d). Two studies of ambient aerosol at urban locations revealed similar average values as compared to the mountain sites with ~~γ(HO$_2$)~~ γ_{HO2} = 0.23 $\pm$ 0.22 in Yokohama, Japan (Zhou et al., 2021) and 0.24 (0.08 ≤ ~~γ(HO$_2$)~~ ≤ γ_{HO2} ≤ 0.36) in Kyoto, Japan (Zhou et al., 2020). No significant trend in the γ values was observed as a function of aerosol or air mass characteristics (coastal or mainland).

Given the large ranges of ~~γ(HO$_2$)~~ γ_{HO2} values on lab-generated and ambient aerosol, it is difficult to reconcile differences

625 between lab data and observations with our model results. However, our results might provide an explanation for the discrepancies of lab-derived or theoretical ~~γ(HO$_2$)~~ γ_{HO2} values in the range of 0.2 - 1 to those determined on ambient aerosol (< 0.4). We cannot say for sure that these differences indeed stem from different assumptions of iron distribution or other factors

affecting ~~$\gamma(HO_2)$~~ γ_{HO2}. However, our strong predicted decrease of ~~$\gamma(HO_2)$~~ γ_{HO2} values at low pH and $F_{N,Fe}$ suggests that applying lab-derived ~~$\gamma(HO_2)$~~ γ_{HO2} on aerosol particles with identical composition might lead to an overestimate of HO_2 loss

630 on atmospheric aerosol surfaces, even if all other aerosol properties (size, total iron mass, pH etc) are identical.

4.3 ROS budgets and oxidative potential (OP)

The formation and cycling of ROS in the aqueous phase is tightly linked to adverse health effects of particulate matter that are caused by oxidative stress in the respiratory tract and lungs (Stohs and Bagchi, 1995; Tong et al., 2017; Molina et al., 2020; Shahpoury et al., 2021). In addition, the oxidant content of ambient aerosol particles controls their ageing time scales and

635 interactions with the biosphere (Pöschl and Shiraiwa, 2015).

Tong et al. (2020) found a positive trend of reactive species concentrations with total particle mass and increased OH concentrations as a function of transition metal content and the opposite trend for organic radicals at remote forest and polluted urban locations. Contrarily, Verma et al. (2012) did not find any correlation of the ROS formation potential with metal concentrations. Fang et al. (2016, 2017) suggested that sulfate may trigger metal solubility in highly acidic supermicron particles, which in turn

640 leads to enhanced ROS formation. On a molar basis, quinones and TMIs may be equally efficient in producing ROS (Charrier and Anastasio, 2012; Lyu et al., 2018); however, as TMI concentrations are higher than those of quinones in aerosol water, TMIs are considered major drivers for ROS levels. In the overview study by Saffari et al. (2014) ROS activity was compared at different locations: at nearly all locations highest activity was observed in $PM_{2.5}$ (as opposed to PM_{10}) samples; this trend was explained with the higher fractions and solubilities of iron in particles of these sizes.

645 Based on such studies, the oxidative potential of atmospheric particulate matter has been related to the presence and amount of TMI in aerosol particles. Our model studies suggest that the total iron amount within an aerosol population may not be a sufficient parameter to constrain the oxidant concentrations within particulate matter ~~. H_2O_2 is often considered one of the main contributors to the total oxidant budget in particles (Tong et al., 2016). Given the large uncertainty in the partitioning of H_2O_2 into aerosol water (Section 3.3.3), the extent is not clear to which the iron distribution affects its total~~

650 ~~concentration in the particles phase. The H_2O_2 budget may be overestimated by up to an order of magnitude if the enhanced Henry's law constant ($K_{Heff,H2O2}$ = $2.7 \cdot 10^8$ M atm^{-1}) is more appropriate (Fig. S4). We find that the OH concentration in particles can be over- or underestimated at low~~ in the atmosphere. However, the resulting health impacts of inhaled particles will likely not be largely affected by $F_{N,Fe}$ ~~, depending on $K_{Heff,H2O2}$ (Fig. S4b), whereas the HO_2 may be overestimated if $K_{Heff,H2O2}$ is higher than the physical Henry's law constant (Fig. S4c). The partitioning of H_2O_2 into aerosol water (i.e.~~

655 ~~$K_{Heff,H2O2}$) is likely dependent on the aerosol composition. Therefore, this dependence together with the ROSdependence on $F_{N,Fe}$ might explain the different conclusions regarding the trends of ROS budgets in particles of different air masses. Similar to the Fe(II)/Fe(III) ratio, our model results suggest that bulk samples of aerosol particles may not accurately represent the ROS budget in ambient populations. Upon sampling, the particles might get dissolved and undergo the ROS formation and conversion processes. Several studies have suggested efficient ROS formation from secondary organic material (e.g.,~~

660 ~~Tong et al. (2018); Zhou et al. (2019); Wei et al. (2021)). The underlying formation processes are not fully clear; given that SOA is likely present in all articles (and droplets), the effect of iron distribution on ROS formation might become less important~~

~~if ROS yields from purely organic particles are sufficiently high. However, it has been shown that ROS formation by SOA can be enhanced in the presence of metal ions (Nguyen et al., 2013; Tuet et al., 2017).~~

While the ROS budgets of atmospheric particulate matter might be different depending on these parameters, these uncertainties might be diminished upon inhalation: Firstly, all iron will be dissolved such that since upon inhalation, iron will likely dissolve in the solution can be described by FeBulk. Secondly, the reaction medium is limited to a bulk liquid phase (lung fluid) andthus H_2O_2 gas lung fluid so that the particle-resolved effects of the iron distribution are diminished. While it may be possible that there are concentration gradients within the lung fluid due to dissolution and/aqueous partitioning does not play a roleor mixing kinetics, such effects cannot be quantified to date.

Generally all conclusions for oxidant budgets in aerosol water also apply to those in cloud water. However, the largest concentration differences for extreme values of $F_{N,Fe}$ are less than an order of magnitude (Section 3.1). Several model studies have explored the sources and production rates of OH in cloud water using chemical mechanisms of different complexities, e.g., Ervens et al. (2003); Deguillaume et al. (2004); Tilgner et al. (2013); Bianco et al. (2015). However, our Our analysis shows that the chemical source and loss rates might be underestimated in bulk cloud water. While the overall oxidant content of the cloud water might not be significantly affected ('bulk aqueous phase concentrations' in Fig. 2 and Fig. 6), the large differences of OH concentrations of about an order of magnitude in iron-containing and iron-free droplets may lead to very different oxidation rates of organics. Higher OH concentrations in the aqueous phase may also lead to more efficient formation of organics acids (aqSOA; Ervens et al. (2011, 2014). Generally highest OH concentrations in cloud water are predicted under clean (marine, remote) conditions (Herrmann et al., 2000; Tilgner et al., 2013). Our results suggest that the difference in OH concentrations might be even greater between low and high pH as we find the largest impact by $F_{N,Fe}$ for high pH. Even though in clean air masses, total iron concentrations might be lower, such trends might be robust as we do not find a strong dependence of the predicted OH concentrations on m_{Fe}. Given the close connections of OH and HO_2/O_2^-, any conclusions for the OH concentrations in cloud water can be similarly drawn also for HO_2/O_2^-. In contrast, the less reactive and more soluble H_2O_2 is not affected by the iron distribution.

5 Summary and conclusions

The role of transition metal ion (TMI) reactions for impacting oxidant levels (OH, HO_2, H_2O_2) in the atmospheric aqueous phase has been recognized for a long time. However, in atmospheric multiphase chemistry models, it usually assumed that all aerosol particles and droplets contain TMI and thus TMI catalyzed reaction TMI-catalyzed reactions occur in all droplets. Single-particle analyses have shown that only a small number fraction of particles contain iron, which implies the same for cloud droplets that are formed on such particles.

Using a box model with a well-established chemical multiphase mechanism, we explored the importance of iron distribution across (i) aqueous aerosol particle or (ii) cloud droplet populations. We performed box model studies in which a constant iron concentration (10 or ng m^{-3}; in sensitivity studies also 50 ng m^{-3}) is distributed to a number fraction $F_{N,Fe}$ of aerosol particles or droplets from 1% to 100% ('FeN<100and FeBulk approaches ' and 'FeBulk' approaches, respectively).

695   We find that H_2O_2 ~~$_2O_2$~~ concentrations in cloud water are not affected by $F_{N,Fe}$ ~~as H_2O_2~~. Its main source and loss processes include the recombination of HO_2 and the reaction with S(IV), respectively. Since the loss process is slower than the uptake from the gas phase and the production in the aqueous phase, H_2O_2 is in thermodynamic equilibrium between the gas phase and all droplets. The same conclusions are drawn for H_2O_2 ~~$_2O_2$~~ partitioning into aerosol water if the same Henry's law constant is applied (~~$K_{H,H2O2}$~~ $K_{H,H2O2}$ = $1.02 \cdot 10^5$ M atm^{-1}). However, since H_2O_2 ~~$_2O_2$~~ has been found to partitioning more efficiently

700   into aerosol than into pure water (~~$K_{Heff,H2O2}$~~ $K_{H,H2O2}$ = $2.7 \cdot 10^8$ M atm^{-1}), We find that H_2O_2 ~~$_2O_2$~~ concentrations in cloud water might be underestimated by the FeBulk approach, whereas it maybe overestimated in aerosol water. These differences are largest at pH = 6 whereas the differences are negligible at pH = 3 or 4.5. The opposite trends are found for the OH radical whose aqueous phase concentration in cloud water might be overestimated by up to a factor of 5 using the FeBulk approach at pH = 6 whereas there might be an over- or underestimate by nearly an order of magnitude in aerosol water, depending on the

705   choice of ~~$K_{Heff,H2O2}$~~ $K_{Heff,H2O2}$.

   The concentrations of OH and HO_2 ~~$_2$~~ radicals are closely linked. Generally we find that the HO_2~~O_2^-~~ ~~$_2$~~/O_2^- concentrations in the aqueous phase are underestimated by the FeBulk approach, again with the largest discrepancies at pH = 6 for $F_{N,Fe}$ = 1% or 100%. This trend can be explained by the increase of the effective Henry's law constant of HO_2 ~~$_2$~~ at high pH (~~$K_{Heff,HO2}$~~ $K_{Heff,HO2}$ = $1.5 \cdot 10^5$ M atm^{-1}) and the higher rate constants of ~~O_2^-~~ the O_2^- radical anion as compared to the corresponding

710   reactions of the HO_2 ~~$_2$~~ radical. The higher partitioning together with the quicker consumption of HO_2~~O_2^-~~ ~~$_2$~~/O_2^- at high pH leads to its subsaturation in the aqueous phase at high pH. This effect is strongest at low $F_{N,Fe}$ because the few iron-containing droplets (particles) are highly concentrated in iron. The reaction of Fe(III) ions or hydroxy complexes with HO_2~~O_2^-~~ ~~$_2$~~/O_2^- is the main sink of HO_2~~O_2^-~~ ~~$_2$~~/O_2^- in both the cloud and aerosol aqueous phases. At the same time it is also the main reduction pathway of Fe(III) to Fe(II). Since the HO_2~~O_2^-~~ ~~$_2$~~/O_2^- concentration in iron-containing droplets is up to one orders of magnitude

715   lower in the FeBulk approach, respectively, the Fe(III) reduction is less efficient. Our results are largely independent ~~form~~ of the total iron mass concentration as both the chemical HO_2~~O_2^-~~ ~~$_2$~~/O_2^- sources and sinks are dependent on iron. Based on these results, we conclude that the Fe(II)/Fe(~~III~~total) ratio in cloud and aerosol water might be lower than implied by bulk samples. This finding has implications on the interpretation of modeled and measured Fe(II)/Fe(~~III~~total) (or Fe(II)/Fe(III)) ratios that are often considered a measure of iron solubility and bioavailability. Our study demonstrates that multiphase chemistry models

720   might not be able to predict properly OH and HO_2 ~~$_2$~~ concentrations in the aqueous phase of cloud or aqueous particle which might translate into biases in the predicted oxidation rates (e.g. aqSOA formation). While not explored in detail in the current study, further implications of iron distribution in cloud droplets might include differences in sulfate formation rates by metal-catalyzed processes.

   The reactive uptake of OH and HO_2 ~~$_2$~~ is often parameterized by γ. We derived γ values into cloud and aerosol water from

725   our model studies. ~~While γ(OH) is~~ The values of γ_{OH} are not largely affected by the iron distribution ~~, γ(HO$_2$~~and show values of $\gamma_{OH} \sim 0.0023$ for clouds and $\gamma_{OH} \sim 0.038$ for aerosol water. ~~,~~ However, γ_{HO2}(aerosol) can be significantly reduced at low $F_{N,Fe}$ as compared to bulk samples, ~~by~~ showing difference of up to two orders of magnitude at pH = 3 (γ(HO$_2$ $\gamma_{HO2} \sim$ ~~0.05 for $F_{N,Fe}$ = 100% and γ(HO$_2$ ~~$\sim$ 0.03 for $F_{N,Fe}$ = 100% and ~~0.0002~~ $\gamma_{HO2} \sim 0.0001$ for $F_{N,Fe}$ = 2%). This analysis demonstrates that γ values that are measured in lab studies using internally mixed aerosol particles might bee too high as compared to those

ambient aerosol populations. In addition to another factors that affect $\gamma(HO_2)$ γ_{HO2} on various aerosol surfaces (chemical composition, particle size, water content etc), our results suggest that also the iron distribution across particle populations can add to the large variability of $\gamma(HO_2)$ γ_{HO2} and to the mismatch of observed and modeled HO_2 loss if lab-derived data are used. Similar considerations can be also applied to the interpretation of ROS formation and oxidative potential of aerosol particles. As ambient aerosol particles likely comprise external mixtures in terms of iron, neither results based on bulk sampling nor on modeling will correctly represent the oxidant budgets in ambient particulate matter.

Our study is to our knowledge the first explicit chemical multiphase model study that systematically explores the role of iron distribution across individual aqueous aerosol particles or cloud droplets for the concentrations and uptake rates of reactive oxygen species. There is only few data available on the iron distribution in aerosol populations form from single-particle analyses, that may be used on constrain the number fraction of iron-containing particles and droplets that contain iron ($F_{N,Fe}$) for clouds and aerosols. While we restricted our model studies to iron, similar conclusions may be also drawn for other transition metal ions, such as copper or manganese. We identified various potential implications of this parameter for e.g. (i) oxidant budgets and particle mass formation (aqSOA, sulfate) in clouds and aerosols, (ii) reactive radical (OH, HO_2) uptake onto aerosols, and (iii) oxidative potentials of aerosol particles that should be further explored by experimental and model studies.

Data availability. The model output is available at https://doi.org/10.5281/zenodo.5829360

Author contributions. BE designed and led the study. AK performed the model studies. AK and BE wrote manuscript; MZ contributed to the discussion of the results.

Competing interests. The authors declare that they have no conflict of interest

Acknowledgements. This work has been supported by the French National Research Agency (ANR) (grant no. ANR-17-MPGA- 0013). We thank Daniel Murphy (NOAA/ESRL) for useful discussion and sharing data of single particle measurements. We thank two anonymous referees whose comments have helped to improve the manuscript.

References

Al-Abadleh, H. A.: Review of the bulk and surface chemistry of iron in atmospherically relevant systems containing humic-like substances, RSC Advances, 5, 45 785–45 811, https://doi.org/10.1039/C5RA03132J, 2015.

755 Alexander, B., Park, R. J., Jacob, D. J., and Gong, S.: Transition metal-catalyzed oxidation of atmospheric sulfur: Global implications for the sulfur budget, J. Geophys. Res. - Atmos., 114, D02 309, https://doi.org/10.1029/2008jd010486, 2009.

Arangio, A. M., Slade, J. H., Berkemeier, T., Pöschl, U., Knopf, D. A., and Shiraiwa, M.: Multiphase Chemical Kinetics of OH Radical Uptake by Molecular Organic Markers of Biomass Burning Aerosols: Humidity and Temperature Dependence, Surface Reaction, and Bulk Diffusion, The Journal of Physical Chemistry A, 119, 4533–4544, https://doi.org/10.1021/jp510489z, 2015.

760 Arangio, A. M., Tong, H., Socorro, J., Pöschl, U., and Shiraiwa, M.: Quantification of environmentally persistent free radicals and reactive oxygen species in atmospheric aerosol particles, Atmos. Chem. Phys., 16, 13 105–13 119, https://doi.org/10.5194/acp-16-13105-2016, 2016.

Barth, M. C., Ervens, B., Herrmann, H., Tilgner, A., McNeill, V. F., Tsui, W. G., Deguillaume, L., Chaumerliac, N., Carlton, A. G., and Lance, S.: Box Model Intercomparison of Cloud Chemistry, Journal of Geophysical Research Atmospheres, 126, e2021JD035 486, 765 https://doi.org/10.1029/2021JD035486, 2021.

Bedjanian, Y., Lelièvre, S., and Le Bras, G.: Experimental study of the interaction of HO2 radicals with soot surface, Phys. Chem. Chem. Phys., 7, 334–341, https://doi.org/10.1039/B414217A, 2005.

Bertram, A. K., Ivanov, A. V., Hunter, M., Molina, L. T., and Molina, M. J.: The reaction probability of OH on Organic Surfaces of Tropospheric Interest, The Journal of Physical Chemistry A, 105, 9415–9421, https://doi.org/10.1021/jp0114034, 2001.

770 Bianchini, R. H., Tesa-Serrate, M. A., Costen, M. L., and McKendrick, K. G.: Collision-Energy Dependence of the Uptake of Hydroxyl Radicals at Atmospherically Relevant Liquid Surfaces, The Journal of Physical Chemistry C, 122, 6648–6660, https://doi.org/10.1021/acs.jpcc.7b12574, 2018.

Bianco, A., Passananti, M., Perroux, H., Voyard, G., Mouchel-Vallon, C., Chaumerliac, N., Mailhot, G., Deguillaume, L., and Brigante, M.: A better understanding of hydroxyl radical photochemical sources in cloud waters collected at the puy de Dôme station – experimental 775 versus modelled formation rates, Atmos. Chem. Phys., 15, 9191–9202, https://doi.org/10.5194/acp-15-9191-2015, 2015.

Chan, M. N., Zhang, H., Goldstein, A. H., and Wilson, K. R.: Role of Water and Phase in the Heterogeneous Oxidation of Solid and Aqueous Succinic Acid Aerosol by Hydroxyl Radicals, The Journal of Physical Chemistry C, 118, 28 978–28 992, https://doi.org/10.1021/jp5012022, 2014.

Chang, J. S., Brost, R. A., Isaksen, I. S. A., Madronich, S., Middleton, P., Stockwell, W. R., and Walcek, C. J.: A three-780 dimensional Eulerian acid deposition model: Physical concepts and formulation, J. Geophys. Res. - Atmos., 92, 14 681–14 700, https://doi.org/10.1029/JD092iD12p14681, 1987.

Charrier, J. G. and Anastasio, C.: On dithiothreitol (DTT) as a measure of oxidative potential for ambient particles: evidence for the importance of soluble transition metals, Atmospheric Chemistry and Physics, 12, 9321–9333, https://doi.org/10.5194/acp-12-9321-2012, 2012.

785 Charrier, J. G., Richards-Henderson, N. K., Bein, K. J., McFall, A. S., Wexler, A. S., and Anastasio, C.: Oxidant production from source-oriented particulate matter - Part 1: Oxidative potential using the dithiothreitol (DTT) assay, Atmospheric Chemistry and Physics, https://doi.org/10.5194/acp-15-2327-2015, 2015.

Che, D. L., Smith, J. D., Leone, S. R., Ahmed, M., and Wilson, K. R.: Quantifying the reactive uptake of OH by organic aerosols in a continuous flow stirred tank reactor, Phys. Chem. Chem. Phys., 11, 7885–7895, https://doi.org/10.1039/B904418C, 2009.

790 Choël, M., Deboudt, K., Flament, P., Aimoz, L., and Mériaux, X.: Single-particle analysis of atmospheric aerosols at Cape Gris-Nez, English Channel: Influence of steel works on iron apportionment, Atmospheric Environment, 41, 2820–2830, https://doi.org/10.1016/j.atmosenv.2006.11.038, 2007.

Christian, K. E., Brune, W. H., and Mao, J.: Global sensitivity analysis of the GEOS-Chem chemical transport model: ozone and hydrogen oxides during ARCTAS (2008), Atmospheric Chemistry and Physics, 17, 3769–3784, https://doi.org/10.5194/acp-17-3769-2017, 2017.

795 Cini, R., Prodi, F., Santachiara, G., Porcu, F., Bellandi, S., Stortini, A., Oppo, C., Udisti, R., and Pantani, F.: Chemical characterization of cloud episodes at a ridge site in Tuscan Appennines, Italy, Atmospheric Research, 61, 311–334, https://doi.org/10.1016/S0169-8095(01)00139-9, 2002.

Cooper, P. L. and Abbatt, J. P. D.: Heterogeneous Interactions of OH and HO_2 Radicals with Surfaces Characteristic of Atmospheric Particulate Matter, The Journal of Physical Chemistry, 100, 2249–2254, https://doi.org/10.1021/jp952142z, 1996.

800 Deguillaume, L., Leriche, M., Monod, A., and Chaumerliac, N.: The role of transition metal ions on HO_x radicals in clouds: a numerical evaluation of its impact on multiphase chemistry, Atmos. Chem. Phys., 4, 95–110, https://doi.org/10.5194/acp-4-95-2004, 2004.

Deguillaume, L., Leriche, M., Desboeufs, K., Mailhot, G., George, C., and Chaumerliac, N.: Transition metals in atmospheric liquid particles: Sources, reactivity and sensitive parameters, Chemical Reviews, 105, 3388–3431, http://pubs.acs.org/doi/pdf/10.1021/cr040649c, 2005.

805 Ervens, B.: Modeling the Processing of Aerosol and Trace Gases in Clouds and Fogs, Chemical Reviews, 115, 4157–4198, https://doi.org/10.1021/cr5005887, 2015.

Ervens, B., George, C., Williams, J. E., Buxton, G. V., Salmon, G. A., Bydder, M., Wilkinson, F., Dentener, F., Mirabel, P., Wolke, R., and Herrmann, H.: CAPRAM2.4 (MODAC mechanism): An extended and condensed tropospheric aqueous phase mechanism and its application, J. Geophys. Res., 108, 4426, https://doi.org/doi: 10.1029/2002JD002202, http://onlinelibrary.wiley.com/doi/10.1029/2002JD002202/abstract, 2003.

810 Ervens, B., Carlton, A. G., Turpin, B. J., Altieri, K. E., Kreidenweis, S. M., and Feingold, G.: Secondary organic aerosol yields from cloud-processing of isoprene oxidation products, Geophysical Research Letters, 35, L02 816, https://doi.org/10.1029/2007gl031828, 2008.

Ervens, B., Turpin, B. J., and Weber, R. J.: Secondary organic aerosol formation in cloud droplets and aqueous particles (aqSOA): a review of laboratory, field and model studies, Atmos Chem Phys, 11, https://doi.org/10.5194/acp-11-11069-2011, 2011.

815 Ervens, B., Sorooshian, A., Lim, Y. B., and Turpin, B. J.: Key parameters controlling OH-initiated formation of secondary organic aerosol in the aqueous phase (aqSOA), J. Geophys. Res. - Atmos., 119, 3997–4016, https://doi.org/10.1002/2013JD021021, 2014.

Fang, T., Verma, V., Bates, J. T., Abrams, J., Klein, M., Strickland, M. J., Sarnat, S. E., Chang, H. H., Mulholland, J. A., Tolbert, P. E., Russell, A. G., and Weber, R. J.: Oxidative potential of ambient water-soluble PM$_{2.5}$ \hack{\newline} in the southeastern United States: contrasts in \hack{\newline} sources and health associations between ascorbic \hack{\newline} acid (AA) and dithiothreitol

820 (DTT) assays, Atmospheric Chemistry and Physics, 16, 3865–3879, https://doi.org/10.5194/acp-16-3865-2016, 2016.

Fang, T., Guo, H., Zeng, L., Verma, V., Nenes, A., and Weber, R. J.: Highly Acidic Ambient Particles, Soluble Metals, and Oxidative Potential: A Link between Sulfate and Aerosol Toxicity, Environmental Science & Technology, 51, 2611–2620, https://doi.org/10.1021/acs.est.6b06151, 2017.

Fomba, K. W., van Pinxteren, D., Müller, K., Iinuma, Y., Lee, T., Collett Jr., J. L., and Herrmann, H.: Trace metal characterization of aerosol particles and cloud water during HCCT 2010, Atmospheric Chemistry and Physics, 15, 8751–8765, https://doi.org/10.5194/acp-15-8751-2015, 2015.

Furutani, H., Jung, J., Miura, K., Takami, A., Kato, S., Kajii, Y., and Uematsu, M.: Single-particle chemical characterization and source apportionment of iron-containing atmospheric aerosols in Asian outflow, J. Geophys. Res. - Atmos., 116, https://doi.org/10.1029/2011jd015867, 2011.

George, I. J., Vlasenko, A., Slowik, J. G., Broekhuizen, K., and Abbatt, J. P. D.: Heterogeneous oxidation of saturated organic aerosols by hydroxyl radicals: uptake kinetics, condensed-phase products, and particle size change, Atmospheric Chemistry and Physics, 7, 4187–4201, https://doi.org/10.5194/acp-7-4187-2007, 2007.

Guo, J., Wang, Z., Tao Wang, and Zhang, X.: Theoretical evaluation of different factors affecting the HO2 uptake coefficient driven by aqueous-phase first-order loss reaction, Science of The Total Environment, 683, 146–153, https://doi.org/10.1016/j.scitotenv.2019.05.237, 2019.

Haggerstone, A.-L., Carpenter, L. J., N., C., and McFiggans, G.: Improved model predictions of HO_2 with gas to particle mass transfer rates calculated using aerosol number size distributions, J. Geophys. Res., 110, https://doi.org/10.1029/2004JD005282, 2005.

Hanson, D. R., Burkholder, J. B., Howard, C. J., and Ravishankara, A. R.: Measurement of hydroxyl and hydroperoxy radical uptake coefficients on water and sulfuric acid surfaces, J. Phys. Chem., 96, 4979–4985, https://doi.org/10.1021/j100191a046, 1992.

Hasson, A. S. and Paulson, S. E.: An investigation of the relationship between gas-phase and aerosol borne hydroperoxides in urban air, J. Aerosol Sci., 34, 459–468, https://doi.org/10.1016/S0021-8502(03)00002-8, 2003.

Herrmann, H., Ervens, B., Jacobi, H.-W., Wolke, R., Nowacki, P., and Zellner, R.: CAPRAM2.3: A Chemical Aqueous Phase Radical Mechanism for Tropospheric Chemistry, J. Atmos. Chem., 36, 231–284, http://link.springer.com/article/10.1023{%}2FA{%}3A1006318622743, 2000.

Houle, F. A., Hinsberg, W. D., and Wilson, K. R.: Oxidation of a model alkane aerosol by OH radical: the emergent nature of reactive uptake, Phys. Chem. Chem. Phys., 17, 4412–4423, https://doi.org/10.1039/C4CP05093B, 2015.

Ingall, E. D., Feng, Y., Longo, A. F., Lai, B., Shelley, R. U., Landing, W. M., Morton, P. L., Nenes, A., Mihalopoulos, N., Violaki, K., Gao, Y., Sahai, S., and Castorina, E.: Enhanced Iron Solubility at Low pH in Global Aerosols, https://doi.org/10.3390/atmos9050201, 2018.

Jacob, D. J.: Heterogeneous chemistry and tropospheric ozone, Atmos. Environ, 34, 2131–2159, https://doi.org/10.1016/S1352-2310(99)00462-8, 2000.

Khaled, A., Zhang, M., Amato, P., Delort, A.-M., and Ervens, B.: Biodegradation by bacteria in clouds: an underestimated sink for some organics in the atmospheric multiphase system, Atmospheric Chemistry and Physics, 21, 3123–3141, https://doi.org/10.5194/acp-21-3123-2021, 2021.

Lakey, P. S. J., George, I. J., Whalley, L. K., Baeza-Romero, M. T., and Heard, D. E.: Measurements of the HO2 Uptake Coefficients onto Single Component Organic Aerosols, Environmental Science & Technology, 49, 4878–4885, https://doi.org/10.1021/acs.est.5b00948, 2015.

Lakey, P. S. J., Berkemeier, T., Krapf, M., Dommen, J., Steimer, S. S., Whalley, L. K., Ingham, T., Baeza-Romero, M. T., Pöschl, U., Shiraiwa, M., Ammann, M., and Heard, D. E.: The effect of viscosity and diffusion on the HO2 uptake by sucrose and secondary organic aerosol particles, Atmos. Chem. Phys., 16, 13 035–13 047, https://doi.org/10.5194/acp-16-13035-2016, 2016.

Li, J. and Knopf, D. A.: Representation of Multiphase OH Oxidation of Amorphous Organic Aerosol for Tropospheric Conditions, Environmental Science & Technology, https://doi.org/10.1021/acs.est.0c07668, 2021.

Li, K., Jacob, D. J., Liao, H., Shen, L., Zhang, Q., and Bates, K. H.: Anthropogenic drivers of 2013 - 2017 trends in summer surface ozone in China, Proceedings of the National Academy of Sciences, 116, 422–427, https://doi.org/10.1073/pnas.1812168116, 2019.

Luo, C., Mahowald, N. M., Meskhidze, N., Chen, Y., Siefert, R. L., Baker, A. R., and Johansen, A. M.: Estimation of iron solubility from observations and a global aerosol model, Journal of Geophysical Research: Atmospheres, 110, https://doi.org/10.1029/2005JD006059, 2005.

Lyu, Y., Guo, H., Cheng, T., and Li, X.: Particle Size Distributions of Oxidative Potential of Lung-Deposited Particles: Assessing Contributions from Quinones and Water-Soluble Metals, Environmental Science & Technology, 52, 6592–6600, https://doi.org/10.1021/acs.est.7b06686, 2018.

Macintyre, H. L. and Evans, M. J.: Parameterisation and impact of aerosol uptake of HO_2 on a global tropospheric model, Atmos. Chem. Phys., 11, 10 965–10 974, https://doi.org/10.5194/acp-11-10965-2011, 2011.

Madronich, S. and Calvert, J. G.: The NCAR Master Mechanism of the Gas Phase Chemistry – Version 2.0, Tech. rep., No. NCAR/TN- 333+STR, University Corporation for Atmospheric Research, https://doi.org/10.5065/D6HD7SKH, http://dx.doi.org/10.5065/D6HD7SKH, 1989.

Mao, J., Fan, S., Jacob, D. J., and Travis, K. R.: Radical loss in the atmosphere from Cu-Fe redox coupling in aerosols, Atmos. Chem. Phys., 13, 509, https://doi.org/10.5194/acp-13-509-2013, 2013.

Mao, J., Fan, S., and Horowitz, L. W.: Soluble Fe in Aerosols Sustained by Gaseous HO2 Uptake, Environmental Science & Technology Letters, 4, 98–104, https://doi.org/10.1021/acs.estlett.7b00017, 2017.

Matthews, P. S. J., Baeza-Romero, M. T., Whalley, L. K., and Heard, D. E.: Uptake of HO_2 radicals onto Arizona test dust particles using an aerosol flow tube, Atmospheric Chemistry and Physics, 14, 7397–7408, https://doi.org/10.5194/acp-14-7397-2014, 2014.

Moffet, R. C., Furutani, H., Rödel, T. C., Henn, T. R., Sprau, P. O., Laskin, A., Uematsu, M., and Gilles, M. K.: Iron speciation and mixing in single aerosol particles from the Asian continental outflow, Journal of Geophysical Research: Atmospheres, 117, https://doi.org/10.1029/2011JD016746, 2012.

Molina, C., Toro A., R., Manzano, C. A., Canepari, S., Massimi, L., and Leiva-Guzmán, M. A.: Airborne Aerosols and Human Health: Leapfrogging from Mass Concentration to Oxidative Potential, https://doi.org/10.3390/atmos11090917, 2020.

Moon, D. R., Taverna, G. S., Anduix-Canto, C., Ingham, T., Chipperfield, M. P., Seakins, P. W., Baeza-Romero, M.-T., and Heard, D. E.: Heterogeneous reaction of HO_2 with airborne TiO_2 particles and its implication for climate change mitigation strategies, Atmospheric Chemistry and Physics, 18, 327–338, https://doi.org/10.5194/acp-18-327-2018, 2018.

Morita, A., Kanaya, Y., and Francisco, J. S.: Uptake of the HO2 radical by water: Molecular dynamics calculations and their implications for atmospheric modeling, J. Geophys. Res. - Atmos., 109, D09 201, https://doi.org/10.1029/2003jd004240, 2004.

Mozurkewich, M., H, M. P., Gupta, A., and Calvert, J. G.: Mass Accommodation Coefficient for HO_2 Radicals on Aqueous Particles, J. Geophys. Res., 92, 4163–4170, 1987.

Myriokefalitakis, S., Ito, A., Kanakidou, M., Nenes, A., Krol, M. C., Mahowald, N. M., Scanza, R. A., Hamilton, D. S., Johnson, M. S., Meskhidze, N., Kok, J. F., Guieu, C., Baker, A. R., Jickells, T. D., Sarin, M. M., Bikkina, S., Shelley, R., Bowie, A., Perron, M. M. G., and Duce, R. A.: Reviews and syntheses: the GESAMP atmospheric iron deposition model intercomparison study, Biogeosciences, 15, 6659–6684, https://doi.org/10.5194/bg-15-6659-2018, 2018.

Nathanson, G. M., Davidovits, P., Worsnop, D. R., and Kolb, C. E.: Dynamics and Kinetics at the Gas-Liquid Interface, J. Phys. Chem., 100, 13 007–13 020, http://pubs.acs.org/doi/pdf/10.1021/jp953548e, 1996.

Nguyen, T. B., Coggon, M. M., Flagan, R. C., and Seinfeld, J. H.: Reactive Uptake and Photo-Fenton Oxidation of Glycolaldehyde in Aerosol
Liquid Water, Environmental Science & Technology, 47, 4307–4316, https://doi.org/10.1021/es400538j, 2013.

Pöschl, U. and Shiraiwa, M.: Multiphase Chemistry at the Atmosphere–Biosphere Interface Influencing Climate and Public Health in the
Anthropocene, Chemical Reviews, 115, 4440–4475, https://doi.org/10.1021/cr500487s, 2015.

Pöschl, U., Rudich, Y., and Ammann, M.: Kinetic model framework for aerosol and cloud surface chemistry and gas-particle in-
teractions – Part 1: General equations, parameters, and terminology, Atmospheric Chemistry and Physics, 7, 5989–6023,
https://doi.org/10.5194/acp-7-5989-2007, 2007.

Remorov, R. G., Gershenzon, Y. M., Molina, L. T., and Molina, M. J.: Kinetics and Mechanism of HO2 Uptake on Solid NaCl, The Journal
of Physical Chemistry A, 106, 4558–4565, https://doi.org/10.1021/jp013179o, 2002.

Renbaum, L. H. and Smith, G. D.: Artifacts in measuring aerosol uptake kinetics: the roles of time, concentration and adsorption, Atmos.
Chem. Phys. Discuss., 11, 7971–8002, https://doi.org/10.5194/acpd-11-7971-2011, 2011.

Roeselová, M., Jungwirth, P., Tobias, D. J., and Gerber, R. B.: Impact, Trapping, and Accommodation of Hydroxyl Radical and
Ozone at Aqueous Salt Aerosol Surfaces. A Molecular Dynamics Study, The Journal of Physical Chemistry B, 107, 12 690–12 699,
https://doi.org/10.1021/jp030592i, 2003.

Saffari, A., Daher, N., Shafer, M. M., Schauer, J. J., and Sioutas, C.: Global Perspective on the Oxidative Potential of Airborne Particulate
Matter: A Synthesis of Research Findings, Environmental Science & Technology, 48, 7576–7583, https://doi.org/10.1021/es500937x,
10.1021/es500937x, 2014.

Schwartz, S. E.: Mass-Transport Considerations Pertinent to Aqueous Phase Reactions of Gases in Liquid-Water Clouds, in: Chemistry of
Multiphase Atmospheric Systems of Multiphase Atmospheric Systems, edited by Jaeschke and W., p. 6, NATO ASI Series, Series G:
Ecological Sciences,, Berlin, Heidelberg, https://doi.org/10.1007/978-3-642- 70627-1_16, 1986.

Seinfeld, J. H. and Pandis, S. N.: Atmospheric Chemistry and Physics, John Wiley & Sons, New York, 1998.

Shahpoury, P., Zhang, Z. W., Arangio, A., Celo, V., Dabek-Zlotorzynska, E., Harner, T., and Nenes, A.: The influence of chemical composi-
tion, aerosol acidity, and metal dissolution on the oxidative potential of fine particulate matter and redox potential of the lung lining fluid,
Environment International, 148, 106 343, https://doi.org/10.1016/j.envint.2020.106343, 2021.

Slade, J. H. and Knopf, D. A.: Heterogeneous OH oxidation of biomass burning organic aerosol surrogate compounds: assessment of
volatilisation products and the role of OH concentration on the reactive uptake kinetics, Phys. Chem. Chem. Phys., 15, 5898–5915,
https://doi.org/10.1039/C3CP44695F, 2013.

Smith, J. D., Kroll, J. H., Cappa, C. D., Che, D. L., Liu, C. L., Ahmed, M., Leone, S. R., Worsnop, D. R., and Wilson, K. R.: The heteroge-
neous reaction of hydroxyl radicals with sub-micron squalane particles: a model system for understanding the oxidative aging of ambient
aerosols, Atmospheric Chemistry and Physics, 9, 3209–3222, https://doi.org/10.5194/acp-9-3209-2009, 2009.

Song, H., Chen, X., Lu, K., Zou, Q., Tan, Z., Fuchs, H., Wiedensohler, A., Moon, D. R., Heard, D. E., Baeza-Romero, M.-T., Zheng,
M., Wahner, A., Kiendler-Scharr, A., and Zhang, Y.: Influence of aerosol copper on HO$_{2}$ uptake: a novel parameterized equation,
Atmospheric Chemistry and Physics, 20, 15 835–15 850, https://doi.org/10.5194/acp-20-15835-2020, 2020.

Stadtler, S., Simpson, D., Schröder, S., Taraborrelli, D., Bott, A., and Schultz, M.: Ozone impacts of gas–aerosol uptake in global chemistry
\hack{\break}transport models, Atmospheric Chemistry and Physics, 18, 3147–3171, https://doi.org/10.5194/acp-18-3147-2018, 2018.

Stohs, S. J. and Bagchi, D.: Oxidative mechanisms in the toxicity of metal ions., Free radical biology & medicine, 18, 321–336,
https://doi.org/10.1016/0891-5849(94)00159-h, 1995.

Takahama, S., Gilardoni, S., and Russell, L. M.: Single-particle oxidation state and morphology of atmospheric iron aerosols, Journal of Geophysical Research: Atmospheres, 113, https://doi.org/10.1029/2008JD009810, 2008.

Taketani, F., Kanaya, Y., and Akimoto, H.: Kinetics of Heterogeneous Reactions of HO2 Radical at Ambient Concentration Levels with $(NH_4)_2SO_4$ and NaCl Aerosol Particles, The Journal of Physical Chemistry A, 112, 2370–2377, https://doi.org/10.1021/jp0769936, 2008.

Taketani, F., Kanaya, Y., Pochanart, P., Liu, Y., Li, J., Okuzawa, K., Kawamura, K., Wang, Z., and Akimoto, H.: Measurement of overall uptake coefficients for HO_2 radicals by aerosol particles sampled from ambient air at Mts. Tai and Mang (China), Atmospheric Chemistry and Physics, 12, 11 907–11 916, https://doi.org/10.5194/acp-12-11907-2012, 2012.

Tan, Z., Hofzumahaus, A., Lu, K., Brown, S. S., Holland, F., Huey, L. G., Kiendler-Scharr, A., Li, X., Liu, X., Ma, N., Min, K.-E., Rohrer, F., Shao, M., Wahner, A., Wang, Y., Wiedensohler, A., Wu, Y., Wu, Z., Zeng, L., Zhang, Y., and Fuchs, H.: No Evidence for a Significant Impact of Heterogeneous Chemistry on Radical Concentrations in the North China Plain in Summer 2014, Environmental Science & Technology, 54, 5973–5979, https://doi.org/10.1021/acs.est.0c00525, 2020.

Thornton, J. and Abbatt, J. P. D.: Measurements of HO_2 uptake to aqueous aerosol: Mass accommodation coefficients and net reactive loss, J. Geophys. Res., 100, doi:–10.1029/2004JD005 402, 2005.

Tilgner, A., Bräuer, P., Wolke, R., and Herrmann, H.: Modelling multiphase chemistry in deliquescent aerosols and clouds using CAPRAM3.0i, Journal of Atmospheric Chemistry, 70, 221–256, https://doi.org/10.1007/s10874-013-9267-4, 2013.

Tong, H., Arangio, A. M., Lakey, P. S. J., Berkemeier, T., Liu, F., Kampf, C. J., Brune, W. H., Pöschl, U., and Shiraiwa, M.: Hydroxyl radicals from secondary organic aerosol decomposition in water, Atmos. Chem. Phys., 16, 1761–1771, https://doi.org/10.5194/acp-16-1761-2016, 2016.

Tong, H., Lakey, P. S. J., Arangio, A. M., Socorro, J., Kampf, C. J., Berkemeier, T., Brune, W. H., Pöschl, U., and Shiraiwa, M.: Reactive oxygen species formed in aqueous mixtures of secondary organic aerosols and mineral dust influencing cloud chemistry and public health in the Anthropocene, Faraday Discussions, 200, 251–270, https://doi.org/10.1039/C7FD00023E, 2017.

Tong, H., Lakey, P. S. J., Arangio, A. M., Socorro, J., Shen, F., Lucas, K., Brune, W. H., Pöschl, U., and Shiraiwa, M.: Reactive Oxygen Species Formed by Secondary Organic Aerosols in Water and Surrogate Lung Fluid., Environmental Science & Technology, 52, 11 642–11 651, https://doi.org/10.1021/acs.est.8b03695, 2018.

Tong, H., Liu, F., Filippi, A., Wilson, J., Arangio, A. M., Zhang, Y., Yue, S., Lelieveld, S., Shen, F., Keskinen, H.-M. K., Li, J., Chen, H., Zhang, T., Hoffmann, T., Fu, P., Brune, W. H., Petäjä, T., Kulmala, M., Yao, M., Berkemeier, T., Shiraiwa, M., and Pöschl, U.: Reactive species formed upon interaction of water with fine particulate matter from remote forest and polluted urban air, Atmospheric Chemistry and Physics Discussions, 2020, 1–40, https://doi.org/10.5194/acp-2020-973, 2020.

Tuet, W. Y., Chen, Y., Fok, S., Gao, D., Weber, R. J., Champion, J. A., and Ng, N. L.: Chemical and cellular oxidant production induced by naphthalene secondary organic aerosol (SOA): effect of redox-active metals and photochemical aging, Scientific Reports, 7, 15 157, https://doi.org/10.1038/s41598-017-15071-8, 2017.

Verma, V., Rico-Martinez, R., Kotra, N., King, L., Liu, J., Snell, T. W., and Weber, R. J.: Contribution of Water-Soluble and Insoluble Components and Their Hydrophobic/Hydrophilic Subfractions to the Reactive Oxygen Species-Generating Potential of Fine Ambient Aerosols, Environmental Science & Technology, 46, 11 384–11 392, https://doi.org/10.1021/es302484r, 2012.

Wang, R., Balkanski, Y., Boucher, O., Bopp, L., Chappell, A., Ciais, P., Hauglustaine, D., Peñuelas, J., and Tao, S.: Sources, transport and deposition of iron in the global atmosphere, Atmospheric Chemistry and Physics, 15, 6247–6270, https://doi.org/10.5194/acp-15-6247-2015, 2015.

Waring, C., King, K. L., Bagot, P. A. J., Costen, M. L., and McKendrick, K. G.: Collision dynamics and reactive uptake of OH radicals at liquid surfaces of atmospheric interest, Phys. Chem. Chem. Phys., 13, 8457–8469, https://doi.org/10.1039/C0CP02734K, 2011.

975   Wei, J., Fang, T., Wong, C., Lakey, P. S. J., Nizkorodov, S. A., and Shiraiwa, M.: Superoxide Formation from Aqueous Reactions of Biogenic Secondary Organic Aerosols., Environmental Science & Technology, 55, 260–270, https://doi.org/10.1021/acs.est.0c07789, 2021.

Xuan, X., Chen, Z., Gong, Y., Shen, H., and Chen, S.: Partitioning of hydrogen peroxide in gas-liquid and gas-aerosol phases, Atmospheric Chemistry and Physics, 20, 5513–5526, https://doi.org/10.5194/acp-20-5513-2020, 2020.

Zhang, G., Bi, X., Lou, S., Li, L., Wang, H., Wang, X., Zhou, Z., Sheng, G., Fu, J., and Chen, C.: Source and mixing state of iron-containing

980   particles in Shanghai by individual particle analysis, Chemosphere, 95, 9–16, https://doi.org/10.1016/j.chemosphere.2013.04.046, 2014.

Zhou, J., Elser, M., Huang, R.-J., Krapf, M., Fröhlich, R., Bhattu, D., Stefenelli, G., Zotter, P., Bruns, E. A., Pieber, S. M., Ni, H., Wang, Q., Wang, Y., Zhou, Y., Chen, C., Xiao, M., Slowik, J. G., Brown, S., Cassagnes, L.-E., Daellenbach, K. R., Nussbaumer, T., Geiser, M., Prévôt, A. S. H., El-Haddad, I., Cao, J., Baltensperger, U., and Dommen, J.: Predominance of secondary organic aerosol to particle-bound reactive oxygen species activity in fine ambient aerosol, Atmospheric Chemistry and Physics, 19, 14 703–14 720, https://doi.org/10.5194/acp-19-

985   14703-2019, https://acp.copernicus.org/articles/19/14703/2019/, 2019.

Zhou, J., Murano, K., Kohno, N., Sakamoto, Y., and Kajii, Y.: Real-time quantification of the total HO2 reactivity of ambient air and HO2 uptake kinetics onto ambient aerosols in Kyoto (Japan), Atmospheric Environment, 223, 117 189, https://doi.org/10.1016/j.atmosenv.2019.117189, 2020.

Zhou, J., Sato, K., Bai, Y., Fukusaki, Y., Kousa, Y., Ramasamy, S., Takami, A., Yoshino, A., Nakayama, T., Sadanaga, Y., Nakashima, Y.,

990   Li, J., Murano, K., Kohno, N., Sakamoto, Y., and Kajii, Y.: Kinetics and impacting factors of HO_2 uptake onto submicron atmospheric aerosols during a 2019 air quality study (AQUAS) in Yokohama, Japan, Atmospheric Chemistry and Physics Discussions, 2021, 1–28, https://doi.org/10.5194/acp-2020-1214, 2021.